International Journal of Pharmaceutics 621 (2022) 121755

Contents lists available at ScienceDirect

International Journal of Pharmaceutics

journal homepage: www.elsevier.com/locate/ijpharm

The topical ocular delivery of rapamycin to posterior eye tissues and the suppression of retinal inflammatory disease

Moutaz Y. Badr [a,b], Abdulrahman A. Halwani [c], Uchechukwu Odunze [a], Malihe Eskandarpour [d], Virginia L. Calder [d], Andreas G. Schätzlein [a,e], Ijeoma F. Uchegbu [a,e,*]

[a] School of Pharmacy, University College London, 29-39 Brunswick Square, London WC1N 1AX, United Kingdom
[b] College of Pharmacy, Umm Al-Qura University, Mecca 24381, Saudi Arabia
[c] School of Pharmacy, King Abdulaziz University, Abdullah Sulayman St, Jeddah 80200, Saudi Arabia
[d] University College London, Institute of Ophthalmology, London EC1V 9EL, United Kingdom
[e] Nanomerics Ltd., 6th Floor, 2 London Wall Place, London EC2Y 5AU, United Kingdom

ARTICLE INFO

Keywords:
RAP
MET
Retina
Chitosan
Experimental autoimmune uveitis

ABSTRACT

Treatment of posterior eye diseases with intravitreal injections of drugs, while effective, is invasive and associated with side effects such as retinal detachment and endophthalmitis. In this work, we have formulated a model compound, rapamycin (RAP), in nanoparticle-based eye drops and evaluated the delivery of RAP to the posterior eye tissues in a healthy rabbit. We have also studied the formulation in experimental autoimmune uveitis (EAU) mouse model with retinal inflammation. Aqueous RAP eye drops were prepared using N-palmitoyl-N-monomethyl-N,N-dimethyl-N,N,N-trimethyl-6-O-glycolchitosan (Molecular Envelope Technology – MET) containing 0.23 ± 0.001% w/v RAP with viscosity, osmolarity, and pH within the ocular comfort range, and the formulation (MET-RAP) was stable in terms of drug content at both refrigeration and room temperature for one month. The MET-RAP eye drops delivered RAP to the choroid-retina with a Cmax of 145 ± 49 ng/g (tmax = 1 h). The topical application of the MET-RAP eye drops to the EAU mouse model resulted in significant disease suppression compared to controls, with activity similar to dexamethasone eye drops. The MET-RAP eye drops also resulted in a reduction of RORγt and an increase in both Foxp3 expression and IL-10 secretion, indicating a mechanism involving the inhibition of Th17 cells and the up-regulation of T-reg cells. The MET-RAP formulation delivers RAP to the posterior eye segments, and the formulation is active in EAU.

1. Introduction

Uveitis is a condition that involves inflammation of the uveal tract (Squires et al., 2017). It is mainly categorized based on the site of the inflammation into anterior, intermediate, posterior, and pan-uveitis. Anterior uveitis is the most common form of the disease, and posterior uveitis constitutes 15%–22% of uveitis cases (Tan et al., 2016). Uveitis is the fifth most common cause of visual loss in the developed world (Durrani et al., 2004; Eskandarpour et al., 2017). The role of $CD4^+$T cells has been demonstrated using the experimental autoimmune uveitis (EAU) model in which inflammation is induced by immunization with retinal peptides (Dick, 1995; Boldison et al., 2014), and effector Th1 and/or Th17 $CD4^+$T cells are mediated in disease development/progression (Eskandarpour et al., 2017; Agarwal and Caspi, 2012). The hallmarks of EAU are the onset of ocular inflammation, disruption of the retinal architecture, and partial to complete destruction of the photoreceptor cell layer, which leads to visual loss (Caspi, 2003). The disease may be clinically scored using a non-invasive advanced retinal imaging approach. The first-line treatments are immunosuppressive drugs (steroids, Cyclosporine (CsA)) that can have serious side effects when given long-term (Uy et al., 2015). Intravitreal ocular implants have thus been approved for use in posterior uveitis, and these include the controlled release of implanted steroids (e.g. Ozurdex, 700 μg) (Ensign et al., 2019), thus minimizing the frequency of treatment.

Rapamycin (RAP) is a specific inhibitor of mTOR, that has been shown to have potent immunosuppressive activity (Powell and Delgoffe, 2010; Li et al., 2014) and RAP has been explored to prevent chronic inflammatory diseases such as uveitis (Nguyen et al., 2018). Intravitreal

Abbreviations: MET, Molecular Envelope Technology.

* Corresponding author at: School of Pharmacy, University College London, 29-39 Brunswick Square, London WC1N 1AX, United Kingdom.
E-mail address: ijeoma.uchegbu@ucl.ac.uk (I.F. Uchegbu).

https://doi.org/10.1016/j.ijpharm.2022.121755
Received 2 February 2022; Received in revised form 25 March 2022; Accepted 14 April 2022
Available online 18 April 2022

RAP (Opsiria) is being developed and the US FDA's acceptance for review of Opsiria was important (FDA's acceptance of Santen's Opsiria marks a milestone for the company, n.d.). These intravitreal approaches carry the risks associated with injectables, such as the risk of endophthalmitis, retinal and vitreous hemorrhage, and retinal detachment (Ensign et al., 2019). Oral RAP has been reported to be effective in non-infectious posterior uveitis (Shanmuganathan et al., 2005). However, gastrointestinal and dermatological side effects have been observed with oral RAP formulations (Shanmuganathan et al., 2005). Effective topical administration of RAP requires the drug to permeate the ocular tissues and locate within retinal tissue. It is our hypothesis that eye drops with a similar level of efficacy to intravitreal dosage forms would offer patient convenience and an improved safety profile. In the first instance we sought to test the ability of our formulation to deliver drug to the retinal tissues. A further objective of the study was to evaluate the effectiveness and mechanism of action of nanoparticulate RAP in a disease model of posterior uveitis.

RAP is practically insoluble in water (aqueous solubility = 2.6 μg/mL), has a high molecular weight (MW 914 Da), and contains no functional groups that may be ionized in the pH range between 1 and 10 (Buech et al., 2007). RAP is extremely hydrophobic with a reported log $P = 5.77$ (Cholkar et al., 2015). To formulate RAP into aqueous eye drops and test these eye drops for the delivery of RAP to the posterior eye tissues, a known non-irritant (Uchegbu et al., 2021), mucoadhesive ocular penetration enhancer - N-palmitoyl-N-monomethyl-N,N-dimethyl-N,N,N-trimethyl-6-O-glycolchitosan (Nanomerics' Molecular Envelope Technology – MET) was used (Qu et al., 2006; Siew et al., 2012; Badr et al., 2021). We also evaluated the polymeric RAP formulation in a posterior uveitis model.

2. Materials and methods

2.1. Materials

RAP powder (MW 914.12 g/mol) was purchased from Cambridge Biosciences (Cambridge, UK). Ascomycin (ASC) powder (MW 792.02 g/mol) was purchased from Generon Ltd. (Slough, UK). MET (DP18DQ19, MW 15 kDa) was supplied by Nanomerics Ltd. (London, UK). Water, Acetonitrile, Methanol, and Formic Acid analytical grade solvents were purchased from VWR (Leicestershire, UK). All other chemicals and reagents used were of analytical grade. For the *in vitro* studies, Statens Seruminstitut Rabbit Cornea (SIRC) and Madin-Darby Canine Kidney (MDCK) cell lines were purchased from LGC standards – ATCC (Teddington, UK). 3-(4,5-dimethylthiazol-2-yl)-2,5-diphenyl-2H-tetrazolium bromide (MTT), Eagle's minimum essential medium, fetal bovine serum, non-essential amino acids, and fluorescein isothiocyanate (FITC) dextran 4-kDa (FD-4) were supplied by Sigma-Aldrich (Gillingham, UK). Penicillin-streptomycin, Sodium pyruvate, and glutaMAX were purchased from Life technologies Ltd. (Paisley, UK). Hanks balanced salt solution was supplied from Fisher Scientific (Loughborough, UK). Sodium caprate (C10) was purchased from Santa Cruz biotechnology (Texas, USA). Transwells with a polycarbonate membrane (pore size = 0.4 μm, surface area = 1.12 cm^2) were obtained from Corning®, VWR International (Leicestershire, UK). For the *in vivo* studies, Interphotoreceptor retinoid-binding protein $(IRBP)_{1\text{-}20}$ peptide (GPTHLFQPSLVLDMAKVLLD) was supplied from Cambridge Peptides (Cambridge, UK). Complete Freund's Adjuvant (CFA) and Pertussis toxin from Sigma-Aldrich (Gillingham, UK). Mycobacterium tuberculosis from Difco Voigt Global Distribution (Kansas, USA). RORγt- R-phycoerythrin (PE) and CD4-Brilliant Ultraviolet 395 nm were obtained from BD Biosciences (Oxford, UK). Interleukin-17 (IL-17) -Brilliant Violet 421 nm and -PE, Forkhead box protein P3 (Foxp3)-FITC, T-box gene expressed in T cells (T-bet) -allophycocyanin and Alexa Fluor 642 nm, IL-10-PE and FITC were all obtained from BioLegend (London, UK).

2.2. Drug formulation studies

A thin-film hydration method was used to encapsulate RAP within the MET nanoparticles. The thin-film hydration method was previously reported to encapsulate tacrolimus within MET nanoparticles (Badr et al., 2021). MET has been used to encapsulate prednisolone for topical ocular delivery (Qu et al., 2006) and encapsulate the hydrophobic drug cyclosporine A (Siew et al., 2012; Uchegbu et al., 2021). RAP powder (2 mg) was dissolved in absolute ethanol (0.2% w/v, 1 mL). MET (15 mg) was dispersed in filtered deionized water (1.5% w/v, 1 mL). Both preparations were mixed and placed in a Savant Vacuum Evaporator (ThermoFisher Scientific, Waltham, USA) at 45 °C and spun under vacuum for 2 h until a thin, dry film was formed. The dry film was rehydrated with glycerol (2.6% w/v, 1 mL) as an isotonicity agent (Heaton et al., 1986) and mixed vigorously for 30 min to disperse the film in the solvent. The mixture was subsequently sonicated using MSE Soniprep 150 sonicator MSE UK Ltd. (London, UK) at 50% of its maximum output for 5 min in an ice bath. The formulation was adjusted to a pH of 7.0 using a calibrated pH meter PHS-W Series Benchtop pH/mV meter from SciQuip Ltd. (Shropshire, UK) with 1.0 M NaOH and a simulated sterile filtration step was carried out using a 0.22 μm polyethersulfone (PES) sterile filter. The formulation was then analyzed for drug content, particle size distribution, zeta potential, viscosity, and osmolarity.

2.2.1. HPLC analysis of RAP

The HPLC method was developed for RAP using an Agilent 1220 infinity chromatographic system fitted with a vacuum degasser, quaternary pump, auto-sampler, column compartment with a thermostat, and an ultraviolet (UV) detector (Agilent Technologies, Berkshire, UK). A gradient method was developed using a mobile phase consisting of (A) phosphoric acid (0.1%), (B) acetonitrile as follows: 70% A (0–3 min), 10% A (3–4 min), 10% A (4–8 min), 70% A (8–9 min). A reversed-phase onyx monolithic C18 (Phenomenex Inc., Torrance, USA) column (100 × 4.6 mm; particle size, 5 μm) was used. The column temperature was maintained at 50 °C, and the UV detector was set at a wavelength of 298 nm. The flow rate was 1.0 mL/min, the injection volume was 10 μL, and the run time was 9 min.

A standard curve was prepared as follows. Briefly, a RAP stock solution was prepared at a concentration of 2 mg/mL in acetonitrile. RAP working solutions were prepared by serially diluting RAP stock solutions into acetonitrile to obtain RAP working solutions at a range of concentrations (0.0625–1.0 mg/mL). For quantifying the RAP content in the formulation, an aliquot of the prepared filtered MET-RAP formulations (100 μL) was diluted with acetonitrile (100 μL) and vortexed before sample injection. Ten μL of the sample was injected, and the RAP concentration was determined by HPLC from the standard curve ($y = 6.7149x + 270.34$, $r^2 = 0.9964$; where y = peak area and x = the RAP concentration).

2.2.2. Stability measurements

The MET-RAP formulation stability was determined by measuring the physicochemical properties over 28 days at different storage temperatures and relative humidities (RH). Formulations were stored at room temperature (25 ± 2 °C / 60 ± 5% RH), refrigeration temperature (5 ± 3 °C) and under accelerated conditions (40 ± 2 °C / 75 ± 5% RH). The storage stability conditions were chosen according to the International Conference on Harmonization (ICH) guidelines (Nezlin, 2003; Niazi, 2003), and the measurements were done in triplicate.

Samples were withdrawn from the stored formulations immediately after preparation and at days 7 and 28 of storage. The samples were analyzed to determine if the encapsulated drug concentration, size distribution, zeta potential, pH, osmolarity, and viscosity were altered on storage. The samples were also visually inspected for any macroscopic changes, including precipitation, turbidity, and color changes. Statistical analysis was performed using two-way ANOVA with Tukeýs post-

test. All data were expressed as mean ± SD. (statistical significance was set at $p < 0.05$).

2.2.3. Particle size and zeta potential measurements

The particle size distribution and zeta potential of the formulation were determined on a Malvern ZetaSizer Nano ZS (Malvern Panalytical, Malvern, UK). The size distribution analysis was performed using dynamic light scattering at a backscattering angle of 173° and a temperature of 25 °C. An aliquot of the sample (100 μL) was placed in a disposable plastic cuvette and subsequently loaded into the instrument without dilution. The particle size was reported as intensity distribution, and the mean size of the individual peaks and their corresponding percentages were determined and recorded as mean ± SD of three independent measurements. The zeta potential was measured by loading an aliquot of the sample (600 μL) into folded capillary cells (zeta cells, polycarbonate cell with gold-plated electrodes; Malvern Instruments, DTS1060C) and zeta potential measured at 25 °C, 40 V. The results were presented as mean ± SD, and the resulting data were analyzed using the DTS (Version 4.2) software, Malvern Instruments Ltd. (Malvern, UK).

Transmission Electron Microscopy (TEM) was carried out using the Philips/FEI CM120 Bio Twin from Philips (Oregano, USA). The MET-RAP formulation was imaged by drying a drop of the formulation on a copper TEM grid (a 300 mesh-fomvar/carbon-coated grid) stained with a drop of uranyl acetate (1% w/v). The dried sample was then imaged under the microscope.

2.2.4. Osmolarity measurements

The osmolarity of the formulation (100 μL) was determined using Roebling Milliosmol Osmometer (Geminibv, Apeldoorn, The Netherlands) coupled with a digital display and a freezing needle. The machine was calibrated before each measurement with 300 mOsm/Kg reference standards solution (Reagecon Diagnostics Ltd., Clare, IE). The measurements were conducted in triplicate.

2.2.5. Viscosity measurements

The viscosity of the formulation was measured using an m-VROC viscometer (Rheosense Inc., San Ramon, USA). Samples (500 μL) were inserted into the measuring cell using a 0.5 mL syringe with extreme care to avoid air bubble formation. The viscosity was measured at different shear rates (1000 s^{-1}, 2500 s^{-1}, 5000 s^{-1}, and 7500 s^{-1}) at 25 °C, and the measurement was conducted in triplicate.

2.2.6. Solid-state analysis

The solid-state analysis of the formulation was carried out on a Miniflex 600, Rigaku (Tokyo, Japan). The formulation was dried by freeze-drying. The X-ray diffraction patterns of the powdered materials were collected over the 2θ range of 5 − 45° at a speed of 5° per minute. Briefly, samples (5 mg) of freeze-dried MET, RAP raw material, MET and RAP raw material physically mixed, and the freeze-dried MET-RAP formulation were added to an XRD plate and analyzed. The data were analyzed using Origin, OriginLab (Northampton, USA).

2.3. Biological in vitro studies

The biological *in vitro* studies were carried out to study the cytotoxicity of MET and the formulation on the SIRC cell line. Also, the effect of MET on paracellular transport was studied on a well-known MDCK monolayer model.

2.3.1. Cytotoxicity study

Statens Seruminstitut Rabbit Cornea cells (SIRC cell line, LGC standards –ATCC, Teddington, UK) were seeded at $1x10^4$ cells per well in 96-well plates and allowed to grow for one day in completed cell growth medium. Cells were then treated with increasing concentrations of MET dispersed in filtered deionized water (14.6×10^{-3} – 7.5 mg/mL, 100 μL per well), MET-RAP formulation (1.9×10^{-3} – 1 mg/mL, 100 μL per well), and RAP dissolved in dimethylsulfoxide (1.9×10^{-2} – 10 μg/mL, 100 μL per well), all diluted with medium. Control groups received treatment with DMSO solution at the same volume and concentration used to prepare the RAP treatments, while the negative control was obtained by treating cells with supplemented cell growth medium. Cells were treated and incubated for 4 h at 37 °C and in a 5% CO_2 environment. After the incubation time, the medium was discarded, followed by washing the cells twice with Dulbecco's phosphate buffer saline (DPBS). A fresh completed medium was then added to the cells, and the cells were then incubated for 24 h to allow for recovery. Subsequently, the medium in the plate was removed and washed twice with DPBS, and the MTT solution (0.5 mg/mL, 200 μL) was added to each well, followed by incubating the cells with the MTT solution for two hours at 37 °C and in a 5% CO_2 environment. Following this incubation period, the MTT solution was gently aspirated. Subsequently, DMSO (200 μL) was added to each well, followed by mixing to ensure complete solubilization of the resulting formazan crystals. The plates were then read on a UV spectrophotometer, SpectraMax M2 (Molecular Devices, Wokingham, UK) at a wavelength of 570 nm, and the IC50 values were determined by comparing the data from the test sample wells to the data obtained from control samples and analyzing the data using GraphPad Prism version 9.0.1 for Windows, GraphPad Software (San Diego, USA).

2.3.2. Permeability study

Transport experiments were conducted to investigate the effect of MET on the transepithelial electrical resistance (TEER). The TEER value was used as a measure of monolayer integrity (Srinivasan et al., 2015). The permeability of the paracellular marker FD-4 (Ye et al., 2015) was assessed, and the permeation enhancer C10 (Krug et al., 2013) was employed as a positive control in the MDCK cell line. Transport studies were carried out using filtered HBSS, supplemented with (4-(2-hydroxyethyl)-1-piperazineethanesulfonic acid - HEPES, 10 mM), and sodium bicarbonate (0.75% v/v), with the pH adjusted to 6.8 and 7.4 with NaOH (1 M). The pH values of 6.8 and 7.4 were chosen as this is the pH comfort range of the eye. MET (2 mg/mL) was prepared by dispersing the polymer in filtered deionized water and diluted with HBSS (1 mL) to provide a working solution (1 mg/mL).

Transwells with a polycarbonate membrane (pore size = 0.4 μm, surface area = 1.12 cm^2) were employed for the transport experiments on MDCK cells. MDCK cells (passage number 7–15) were grown on 12 transwells with permeable support using supplemented growth medium for five days. Cells were seeded on transwells at a density of $5x10^5$ cells per well and cultured according to standard protocols (Cho et al., 1989). Briefly, cells with medium (0.5 mL) in the apical compartment and medium (1.5 mL) in the basolateral compartment were allowed to grow and differentiate on the transwells for five days at 37 °C, and 5% CO_2 before the experiment was conducted. The cell culture medium in both chambers was changed every day for the MDCK cells. The TEER measurements were taken regularly using a MILLIPORE Millicell®-ERS voltohmmeter (Merck Millipore, Watford, UK). All TEER and transport experiments were carried out in triplicate.

On the day of the experiment, the cell culture medium was removed, the monolayers rinsed twice with HBSS and then incubated for one hour with HBSS (0.5 mL) at 37 °C, before taking a baseline TEER measurement. Subsequently, HBSS in the apical chamber was removed, and MET, blank HBSS (as a negative control), and sodium caprate (Krug et al., 2013) (10 mM, as a positive control) were added to the apical chamber (0.5 mL). The cells were then incubated for two hours at 37 °C and 5% CO_2, and the after-treatment TEER was measured. Following treatment, both the apical and basolateral chambers were washed once with HBSS. HBSS (1.5 mL) was then added to the basolateral chamber, and filtered FD-4 in HBSS buffer (1 mg/mL, 0.58 mL) was added to the apical chamber. Samples (80 μL) were taken immediately at the beginning of the experiment from the apical chamber to calculate the initial donor concentration (C_0) and at the end of the experiment to facilitate mass balance calculations. The plates were then incubated for two hours

at 37 °C and 5% CO_2, and samples (250 μL) were taken from the basolateral chamber at 30-minute intervals. The samples taken were replenished with an equal volume of HBSS, and the TEER measurement was taken after incubation with FD-4. Later, the FD-4 was removed, and the cells were washed once with HBSS and once with the cell culture medium. The medium was then added to both chambers, and the cells were incubated at 37 °C and in 5% CO_2 to allow for recovery.

Samples taken from the apical and basolateral chambers were placed in black 96 well-plates covered with foil and analyzed using a BioTek Synergy™ HT Multi detection microplate reader (SpectraMax M2, Molecular Devices, Wokingham, UK) at an excitation wavelength of 485 nm and an emission wavelength of 528 nm (Watson et al., 2015). The apparent permeability coefficient (Papp) in cm/s of FD-4 was calculated using the following equation:

$$P_{app} = \frac{dQ}{dt}\frac{1}{AC} \quad (1)$$

where, dQ/dt is the rate of change of concentration in the basolateral chamber over time, A is the surface area of the cell monolayer, C is the initial concentration in the apical chamber. The concentration of the collected samples was determined from a freshly prepared standard curve of FD-4. Statistical data analysis was performed with two-way ANOVA followed by Tukey's multiple comparison test using GraphPad Prism version 9.0.1 for Windows, GraphPad Software (San Diego, USA). The value $p < 0.05$ was considered significant, and the measurements were done in triplicate from three independent experiments.

2.4. Biological in vivo studies

2.4.1. Pharmacokinetics study

New Zealand white male rabbits (n = 12) weighing between 2.0 and 3.0 kg were obtained from Envigo (Huntingdon, UK) and were acclimatized for at least seven days before the experiment. The rabbits had free access to water and food with 12 h of light/dark cycles throughout the study. Treatment of animals conformed to the Association for Research in Vision and Ophthalmology statement for the use of animals in ophthalmic and vision research. All animal studies were ethically reviewed by the local ethics committee and the studies performed in accordance with the UK Animals (Scientific Procedures) Act 1986.

2.4.2. Bioanalytical LC-MS/MS assay

2.4.2.1. Preparation of working standard solutions. RAP stock solution was prepared at a concentration of 100 μg/mL in methanol (MeOH). RAP working stock solutions were prepared by serially diluting RAP stock solutions into MeOH to obtain RAP working stock solutions at a range of concentrations (0.0167–33.4 μg/mL). RAP working standards were prepared by serially diluting RAP working stock solutions into MeOH to obtain the RAP working standards ranging from a concentration (0.5–1000 ng/mL). Ascomycin was used as the internal standard (IS). The IS stock solution was freshly prepared at a concentration of 100 ng/mL in methanol.

2.4.2.2. Preparation of standard and quality control curves. Working standard solutions were prepared to obtain an individual standard curve in each of the rabbit eye blank tissues (cornea, conjunctiva, sclera, choroid-retina, aqueous humor, and vitreous humor). Tissues were homogenized according to the following protocol. Briefly, the solid frozen tissue was cut into small pieces with scissors and ground to a fine powder with a mortar and pestle placed in dry ice, and the absolute tissue mass was weighed (30 mg). Aqueous samples (aqueous humor, vitreous humor, 30 μL) were transferred into a sterile polypropylene tube, and the absolute mass was weighed. Normal saline (470 μL) was added, and samples were vortex-mixed for 5 min. The mixtures were then homogenized using probe sonication (model Q700) from Qsonica LLC (Newtown, USA) at 50% of its maximum output for 25–50 s in an ice bath. The homogenized samples were spiked with RAP working standards (50 μL) in order to generate the standard curves. Also, samples were spiked with the internal standard ascomycin in MeOH (100 ng/mL, 60 μL). Methanol (1060 μL) was added to precipitate the proteins.

The quality control standard curves were generated to evaluate the recovery rate and the matrix effect on drug extraction. Blank samples were prepared similarly to tissue standard curves. Briefly, RAP working standard samples (50 μL) were added to normal saline (500 μL) to generate the standard curves. Samples were spiked with ascomycin in MeOH (100 ng/mL 60 μL). Methanol (1060 μL) was added to mimic the extraction protocol.

The mixtures were then vortexed for 5 min and centrifuged (5000 g × 10 min at 4 °C, Hettich Mikro 200R, Tuttlingen, Germany). An aliquot (1 mL) of the centrifuged homogenate supernatant was evaporated to dryness within the speed vac at 45 °C and spun under vacuum in the evaporator for at least 2 h. The residue was reconstituted in the LC-MS/MS mobile phase (100 μL) and vortex-mixed for 5 min. The sample was once again centrifuged (2000 g × 2 min at 4 °C) to precipitate any tissues. Following this, the sample (80 μL) was transferred to HPLC vials. Ten μL of the reconstituted sample was injected into the LC-MS/MS system.

2.4.2.3. Chromatography. Samples were analyzed using an Agilent 6400 Series Triple Quadrupole LC/MS system (Agilent Technologies, Berkshire, UK) comprising a degasser (HiP Degasser 1260/G4225A), a binary pump (HiP 1260 binary pump/G1312B), an autosampler (HiP sampler 1260/ G1367E), a column oven (G1316A) and a triple-quadrupole mass spectrometer (G6460A). An Agilent MassHunter Workstation Software was used for system control, data acquisition, and data processing.

A sensitive LC-MS/MS method was used to determine the concentration of RAP in the eye tissue homogenates and blank tissue samples. Samples (10 μL) were chromatographed over an XBridge BEH C8 XP column (2.5 μm, 2.1 mm X 50 mm), equipped with a Vanguard Cartridge Holder (part number: 186007949) from Waters Limited (Herts, UK) at a temperature of 50 °C and with the mobile flow rate of 0.5 mL/min. The run time was 6 min, followed by a 1-minute post-run time. The gradient mobile phase was (A) formic acid (0.1% v/v) in water and (B) formic acid (0.1% v/v) in acetonitrile (all were LC-MS grade solvents) as follows: 60% A (0 – 1 min), 5% A (1 – 3 min), 5% A (3 – 5 min), 60% A (5 – 6 min). RAP and ascomycin were monitored by positive electrospray ionization on an Agilent jet stream ion source with ionization source parameters as outlined (Table 1). Samples were scanned using multiple reaction monitoring mode for transitions of RAP *m/z* [M + Na]+ (936.4 → 409.1), and for ascomycin *m/z* [M + Na]+ (814.2 → 604.1), respectively.

2.4.3. MET-RAP animal dosing

Twenty-five μL of the MET-RAP 0.2% w/v formulation was administered to both eyes. Briefly, the lower eyelid was gently pulled away from the eye globe and using a calibrated micropipette, 25 μL of the

Table 1
LC-MS/MS source parameters for RAP and ascomycin.

Parameter	RAP (Analyte)	Ascomycin (Internal standard)
Capillary voltage (V)	3500	3500
Gas temperature (°C)	300	300
Gas flow (L/min)	5	5
Sheath gas heater (°C)	250	250
Sheath gas flow (L/min)	11	11
Nebulizer (psi)	45	45
Fragmentor (V)	200	300
Collision energy (V)	65	45
Precursor ion (*m/z*)	936.4	814.2
Product ion (*m/z*)	409.1	604.1

formulation was applied in the lower conjunctival cul-de-sac. After dosing, the upper and lower eyelids were hand-held together for approximately 5 s to permit the formulation to come into contact with the cornea. The number of blinks in the next 60 s was recorded. Subsequently, after predetermined time points (1, 2, 4, 24 h, n = 3 each), the rabbit was culled with an intravenous injection of 20% w/v phenobarbital (5 mL) through the marginal ear vein using a 25-gauge butterfly needle.

The eye globe was enucleated using sterilized scissors, washed twice with 0.9% w/v normal saline, and dried on a filter paper. Subsequently, the various tissues were dissected, rinsed twice with 0.9% w/v normal saline, and dried on a filter paper. The eye tissues were harvested in the following order to minimize cross-contamination: conjunctiva, aqueous humor, vitreous humor, lens, iris/ciliary body, cornea, choroid-retina, sclera. The harvested dried tissues were immediately stored in ice (2–5 h after dissection) and eventually stored at −80 °C until further analysis could be performed. The aqueous humor was withdrawn using a 26-gauge needle attached to a 2 mL syringe, while vitreous humor was aspirated using a 23-gauge needle attached to a 2 mL syringe. All tissue dissections were performed using sterilized tools. Disposable scalpels, tweezers, and scissors were used as necessary. Any other sharp tools were disinfected with 70% ethanol and washed with 0.9% w/v normal saline before moving to the following tissue. All excised tissues were rinsed twice with 0.9% w/v normal saline before being added to a pre-weighed tube.

For RAP extraction, the tissues were homogenized as described above, and a volume of the tissue homogenates (500 μL) and aqueous samples (aqueous humor and vitreous humor) were used. Briefly, to extract RAP, the protein precipitation method was used. To all the tissue homogenates, an aliquot of the IS in methanol (100 ng/mL, 60 μL) was added and vortexed for 5 min. Methanol (1110 μL) was added to precipitate the proteins and extract RAP. Mixtures were then vortexed for 5 min and centrifuged (5000 g × 10 min at 4 °C). Aliquots (1 mL) of the centrifuged homogenate supernatant were evaporated to dryness within the speed vac at 45 °C and spun under the vacuum evaporator for at least 2 h. The residues were reconstituted in the LC-MS/MS mobile phase (100 μL) and vortex-mixed for 5 min. The samples were again centrifuged (2000 g × 2 min at 4 °C) to precipitate any tissues. Aliquots of the resulting supernatants (80 μL) were transferred to HPLC vials. Ten μL of the reconstituted samples were injected into the LC-MS/MS system.

2.4.4. MET-RAP animal pharmacodynamic study in C57BL/6J mice

Female, 6–8-week-old C57BL/6J mice (n = 20) weighing between 18.0 and 20.0 g were used for the pharmacodynamics study. Animals were obtained from Charles River (Harlow, UK) and were acclimatized for at least seven days before the experiment. All animals had free access to water and food with 12 h of light/dark cycles for the duration of the experiment. Treatment of animals conformed to the Association for Research in Vision and Ophthalmology statement for the use of animals in ophthalmic and vision research (The Association for Research in Vision and Ophthalmology- Statement for the Use of Animals in Ophthalmic and Vision Research, n.d.). All animal studies were ethically reviewed by the local ethics committee, and experiments were performed in accordance with the Animals (Scientific Procedures) Act 1986 and under a Home Office project license.

2.4.4.1. Experimental autoimmune uveitis. Experimental autoimmune uveitis was induced as previously described (Eskandarpour et al., 2017; Boldison et al., 2014). Briefly, mice were immunized with a subcutaneous injection (200 μL) of $IRBP_{1\text{-}20}$ peptide in PBS (300 μg/100 μL) emulsified with CFA and supplemented with *Mycobacterium tuberculosis* (1.5 mg/mL, 100 μL). Mice also received an intraperitoneal injection of pertussis toxin (0.4 μg/100 μL). Animals were housed under specific pathogen-free conditions. Upon arrival, all mice (n = 20) were housed in individually vented cages in a group of five animals in four separate cages. The untreated control group received topical normal saline (pH = 7.4) as a negative control. The MET polymer (0.75% w/v dispersed in 2.6% w/v glycerol in water, pH = 7.4) was topically applied as vehicle control. The clear aqueous formulation MET-RAP (0.2% w/v, pH ~ 7.0–7.4) was topically applied as the treatment group. A commercial preparation of dexamethasone suspension Maxidex (DEX, 0.1% w/v) from Alcon (Camberley, UK) was applied topically as a positive control. All animals received treatment twice a day (5 μL) for seven days after signs of EAU was observed, using fundoscopy on day 13 post-immunization.

2.4.4.2. Clinical scoring. Mice were assessed for early signs of EAU by fundoscopic observation using a Micron III fundus camera, Phoenix Research Labs (Pleasanton, USA). Images were scored from one to five by two blinded experienced independent observers and scored according to the criteria for EAU scoring, based on the level of the immune cell infiltration and the degree of retinal damage, as previously described (Gegg et al., 2005) before and after treatment at days 13, and 20 post-immunization, respectively.

2.4.4.3. Retinal immunophenotyping by flow cytometry. Anti-mouse antibodies were used for retinal cell flow cytometry. Briefly, retinal layers from enucleated eyes were collected at day 20 post-immunization, minced, and filtered to remove any debris and then resuspended in FACS buffer (eBioscience, Hatfield, UK) for cell surface marker staining. Retinal cells isolated for flow cytometry were collected to study the effect of treatments on immune cells. The level of intracellular expression of RORγt/IL-17 was determined to detect the percentage of T-helper 17 (Th17) cells in the sample. In addition, the level of expression of T-bet was determined to detect the percentage of T-helper 1 (Th1) and the level of expression of IL-10 as a regulatory cytokine in foxp3 + Treg cells was also determined.

Flow cytometry data were acquired using LSRFortessa, BD Biosciences (San Jose, USA), BD FACSDiva version 6.1.3 software. Statistical data analysis was performed with one-way ANOVA followed by Kruskal-Wallis multiple comparison test using GraphPad Prism version 9.0.1 for Windows, GraphPad Software (San Diego, USA). The value $p < 0.05$ was considered significant.

3. Results and discussions

3.1. HPLC analysis of RAP

A reverse-phase HPLC method was developed and used to quantify RAP drug content in the formulation. A calibration curve was constructed by plotting the average peak area of RAP areas against concentration. The method developed showed linearity of RAP in a concentration range (62.5–1000 μg/mL). The straight-line equation ($y = 6.7149x + 270.34$, $r^2 = 0.9964$) was used to quantify the concentration of the encapsulated RAP in the formulation. The measured lower limit of quantification for RAP was 62.5 μg/mL. The calculated limit of detection and limit of quantification were 58.8 μg/mL, and 178.1 μg/mL, respectively.

3.2. Drug formulation and stability studies

We manufactured 0.2% w/v RAP eye drops. The solvent evaporation method approach utilizing the MET polymer was used to formulate the lipophilic drug RAP. The level of palmitoylation and quaternization (mole%) of MET can be altered to meet the specific requirements of the formulation (Chooi et al., 2014). In this study, we chose MET with levels of palmitoylation (18%) and quaternization (20%) to balance the lipophilicity and hydrophilicity of the polymer.

The stability of the MET-RAP formulations was determined by measuring their physicochemical properties over 28 days. Table 2 shows

Table 2
Parameters of MET-RAP stored at the fridge (5 ± 3 °C), room temperature (25 ± 2 °C), and at an accelerated condition (40 ± 2 °C) for 28 days.

Storage conditions	Parameters	Day 0	Day 7	Day 28
5 ± 3 °C	Drug concentration (mg/mL)	2.3 ± 0.01	2.6 ± 0.02 #	2.5 ± 0.01 #
	pH	7.2 ± 0.10	6.9 ± 0.04 #	6.9 ± 0.04 #
	Main peak size (nm) Peak intensity (%)	174 ± 2.2 (66 ± 0.4%)	217 ± 23.1 ns (36 ± 4.3%)	411 ± 18.7 ns (35 ± 1.1%)
	Second peak size (nm) Peak intensity (%)	14 ± 1.2 (33 ± 0.8%)	18 ± 3.01 ns (64 ± 4.3%)	14 ± 7.7 ns (45 ± 18.02%)
	Zeta potential (mV)	+26 ± 4.7	+14 ± 2.4 #	+5 ± 0.6 #
	Osmolarity (mOsm/kg)	322 ± 5.5	331 ± 10.02 ns	326 ± 7.6 ns
	Viscosity (mPa.s)	1.4 ± 0.01	1.6 ± 0.03 #	1.4 ± 0.001 ns
25 ± 2 °C 60 ± 5% RH	Drug concentration (mg/mL)	2.3 ± 0.01	2.5 ± 0.02 #	2.4 ± 0.04 ns
	pH	7.2 ± 0.10	6.7 ± 0.03 #	6.7 ± 0.10 #
	Main peak size (nm) Peak intensity(%)	174 ± 2.2 (66 ± 0.4%)	276 ± 30.9 ns (28 ± 3.9%)	665 ± 169.2 # (40 ± 5.3%)
	Second peak size (nm) Peak intensity (%)	14 ± 1.2 (33 ± 0.8%)	24 ± 6.6 ns (61 ± 15.2%)	29 ± 7.3 * (39 ± 12.6%)
	Zeta potential (mV)	+26 ± 4.7	+15 ± 1.4 #	+5 ± 0.4 #
	Osmolarity (mOsm/kg)	322 ± 5.5	332 ± 6.1 ns	329 ± 3.6 ns
	Viscosity (mPa.s)	1.4 ± 0.01	1.6 ± 0.1 #	1.4 ± 0.01 ns
40 ± 2 °C 75 ± 5% RH	Drug concentration (mg/mL)	2.3 ± 0.01	2.3 ± 0.01 ns	1.9 ± 0.02 #
	pH	7.2 ± 0.10	6.8 ± 0.10 #	6.5 ± 0.04 #
	Main peak size (nm) Peak intensity (%)	174 ± 2.2 (66 ± 0.4%)	395 ± 85.5 ns (15 ± 1.6%)	766 ± 244.2 # (11 ± 2.5%)
	Second peak size (nm) Peak intensity (%)	14 ± 1.2 (33 ± 0.8%)	25 ± 1.9 ns (86 ± 1.6%)	31 ± 4.7 # (77 ± 20.01%)
	Zeta potential (mV)	+26 ± 4.7	+18 ± 2.5 ns	+16 ± 1.4 *
	Osmolarity (mOsm/kg)	322 ± 5.5	324 ± 9.3 ns	322 ± 5.5 ns
	Viscosity (mPa.s)	1.4 ± 0.01	1.7 ± 0.03 #	1.4 ± 0.01 ns

ns = not significant; * = $p < 0.05$; # = $p < 0.005$.

the properties of all formulations upon storage at different conditions over 28 days. The formulation stored in the fridge (28 days, 2.5 mg/mL) displayed a similar drug content compared to formulations stored in the fridge at day 0 (2.3 mg/mL) and day 7 (2.6 mg/mL). Formulations stored at room temperature (25 ± 2 °C / 60 ± 5% RH) showed no significant differences in drug content at day 28 when compared to day 0 ($p > 0.05$). MET-RAP stored at accelerated conditions (40 ± 2 °C / 75 ± 5%) showed no significant change in drug content at day 7 when compared to day 0, while the change in drug content was significant at day 28 when compared to day 0 ($p < 0.05$) with 82.60% of the drug remaining in the formulation by day 28. The pH of all the prepared formulations was examined. The pH of the formulation was adjusted to 7.2 ± 0.1 with 1.0 M NaOH. The optimum pH for eye drops equals that of tear fluid and is 7.4 (Baranowski et al., 2014). Our results showed that the pH was in the acceptable range at all conditions and time points for all formulations (pH = 6.7 – 7.2). The particle size and zeta potential were determined for the formulations. The formulation prepared for the stability study possessed two nanoparticle populations after filtration. The main peak population with larger particle sizes (~174 nm) was presumed to be the encapsulated RAP in the formulation. In contrast, the second peak population with smaller particle sizes (~14 nm) was assumed to be empty MET micelles, as reported previously (Badr et al., 2021; Ahmad et al., 2010). It has been reported that in aqueous environments, MET self-assembles to form polymeric micelles with a particle size of between 5 and 30 nm (Serrano et al., 2015). Our size distribution results in the stability studies showed a bimodal distribution, and this bimodal size is thought to be due to an equilibrium being established between drug-filled nanoparticles and empty micelles (Serrano et al., 2015). There were no significant differences in the formulation particle size at day 0 to day 7 of storage at all conditions and time points. The formulation particle size stored in the fridge on day 28 was not significantly different ($p > 0.05$) from the formulation's particle size on day 0. However, there was a significant difference in the formulation particle size when stored at room temperature and at accelerated conditions (40 °C) when day 28 was compared to day 0. Despite these size distribution changes the formulation did not show any visible signs of sedimentation or a loss of drug content when stored at room temperature or below.

To further examine the characteristics of the formulation, electron microscopy was used to observe the morphology of the nanoparticles formed using the MET polymer. Fig. 1 shows that the MET-RAP formulation formed spherical nanoparticles, which are presumed to contain the encapsulated RAP.

MET possesses an overall positive charge due to the presence of quaternary ammonium groups (Lalatsa et al., 2012). As such, we obtained a positive zeta potential with the MET-RAP formulation (+26 ± 4.7 mV) on day 0 over three independent experiments. There were no significant changes in the measured zeta potential on day 28 compared to day 0, irrespective of the storage conditions ($p > 0.05$). The tears have a tonicity equivalent to 0.9% w/v NaCl solution (300 mOsm/L) (Strandvik, 2009; Iyamu and Enobakhare, 2019). Our formulation has an osmolarity value of 322 – 332 mOsm/kg, within the range tolerable by the eye, and the change in osmolarity was not significant, irrespective of the storage conditions ($p > 0.05$). The viscosity of the formulation was measured. The viscosity of the formulation is higher than that of plain water (1.4 mPa versus 0.89 mPa.s (Korson et al., 1969), respectively at 25 °C) due to the presence of the MET polymer in the formulation (Qu et al., 2006). There were no significant changes in the viscosity at day 28

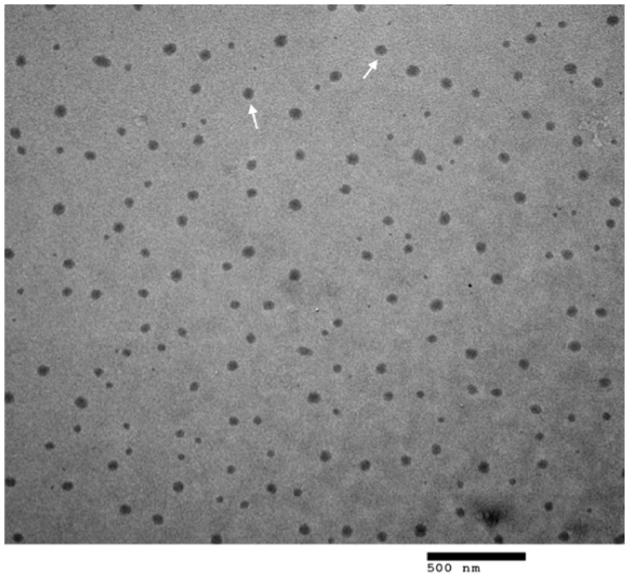

Fig. 1. Transmission electron microscopy image of MET-RAP formulation. The image showed spherical nanoparticles that are presumed to contain the encapsulated rapamycin in the MET-RAP formulation.

compared to day 0, irrespective of the storage conditions ($p > 0.05$). As this formulation is intended for topical ocular administration in the eye, the slightly increased viscosity and the MET bioadhesive properties are important for promoting drug residence time at the ocular surface.

Different approaches have been reported to achieve aqueous incorporation of RAP, including; the use of microemulsions (Buech et al., 2007), and the formulation as solid dispersions (Cho et al., 2015). The incorporation of 1 mg/mL of RAP in an aqueous-based formulation was achieved with a microemulsion containing triacetin and propylene glycol (Buech et al., 2007). The aqueous incorporation of RAP (196.7 μg/mL) was achieved when RAP was spray-dried with polymethacrylate-based copolymers (Eudragit®) due to the formation of micelle-like structures (Cho et al., 2015). RAP at an aqueous level of 1 mg/mL was achieved when amphiphilic block copolymer micelles of polyethylene glycol-b-poly(e-caprolactone) were used (Forrest et al., 2006). Another report showed a RAP-loaded mixed nanomicellar formulation, i.e., vitamin E tocopherol polyethylene glycol succinate and octoxynol-40 led to high RAP aqueous concentrations (2 mg/mL) (Cholkar et al., 2015). All these approaches used high levels of excipients, e.g., a viscosity enhancer povidone K 90 was used, triacetin (20%), and propylene glycol (40%) to enhance RAP levels in eye drop formulations. Our work showed that MET alone at a concentration of 0.75% w/v was able to achieve a high concentration of RAP (0.23% w/v) in our aqueous formulation. MET increased the RAP levels in the aqueous formulation by 1000-fold (from 2.6 μg/mL for RAP alone to 2300 μg/mL for the MET-RAP formulation). We have shown that RAP, when encapsulated with the amphiphilic MET, exhibits excellent stability over 28 days of storage at 5 °C and room temperature, and this stability was due to the formation of larger polymeric drug-filled nanoparticles and micelles. Siew et al. reported that the MET CMC values to range from 21 to 26 μM (Siew et al., 2012). Qu et al. showed that the MET CMC values are between 6 and 100 μM (Qu et al., 2006). This low CMC value makes the MET a prime candidate for use in drug delivery. Highly stable nanosystems will be less likely to disaggregate on dilution within biological fluids *in vivo* prematurely, and as a result, will be able to transport their payload as intended (Siew et al., 2012).

3.3. Solid-state analysis

XRD patterns of tested compounds are presented in (Fig. 2). MET displays no distinct visible Bragg reflections; this demonstrates that MET is an amorphous material. The RAP raw material has sharp peaks; this confirms the plain drug to be a crystalline material, consistent with the literature (Kim et al., 2011). The physical mixture of the freeze-dried MET and RAP raw material still shows some crystalline peaks. In the case of the MET-RAP freeze-dried formulation, the reflections of RAP crystals have disappeared, and therefore the formulation comprises an amorphous solid dispersion. This represents an advantage, as the amorphous form of the drug often has rapid dissolution and greater absorption compared to their crystalline forms. This is important for eye drop formulations as amorphous pharmaceutical materials may lead to enhanced drug solubility in eye drop formulations when compared to their crystalline drug (Hancock and Parks, 2000) and thus contributes to the stability of the formulation. The two peaks at about 40° in all the spectra are due to the plates' background reflections.

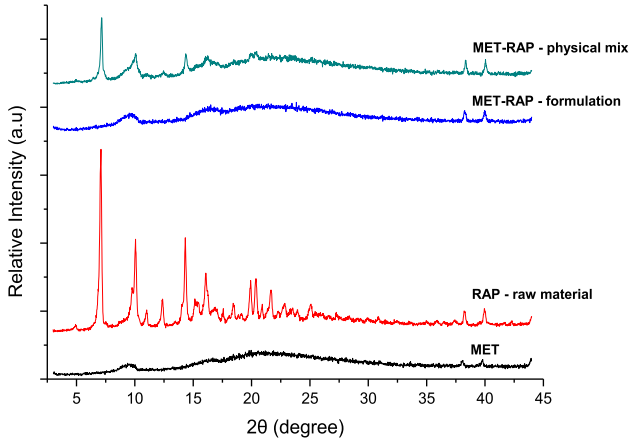

Fig. 2. X-Ray Diffraction analysis of the MET-RAP formulation as compared to MET and RAP raw materials.

3.4. Biological in vitro studies

3.4.1. Cytotoxicity study

The IC50 values of treatment groups were obtained from the relevant dose–response curves. Fig. 3 shows the IC50 values for the MET polymer, MET-RAP formulation, and RAP on the SIRC cell line. MET polymer with high DQ18% and high DP20% has an IC50 of 632.9 ± 48.9 μg/mL. MET is a polycation polymer that has a positive charge that might destabilize the cell membrane to a certain extent and cause cytotoxicity even in the absence of the drug (López-Dávila et al., 2016). The formulation has an IC50 value of 23.69 ± 2.76 μg/mL, while RAP has an IC50 value of 3.77 ± 0.59 μg/mL. Milani et al. reported that RAP did not show toxicity at concentrations 0.1–10 μg/mL using the MTT assay in a human corneal fibroblast culture (Milani et al., 2013). RAP binds to the immunophilin, FK binding protein to interact with mTOR and inhibits its function, leading to cell growth inhibition (Dutcher et al., 2004). The exact effect of how RAP reduced the metabolic activity of the SIRC cell line has not been evaluated. RAP has been approved for the prophylaxis of organ rejection in patients aged ≥ 13 years receiving renal transplants (FDA, 2010). Further studies are needed to define precisely the role of RAP on the inhibition of cell growth in the SIRC cell line. To our knowledge, this is the first data reporting the IC50 value of RAP on the SIRC cell line. The formulation reduces the toxicity of the drug, and this could mean that non-target tissues on the surface of the eye may be less likely to be affected by the drug. Our results demonstrated the good biocompatibility of the MET polymer and the formulation compared to RAP alone against the rabbit cornea cell line.

3.4.2. Permeability study

The development of tight junctions in MDCK cells at pH = 6.8 and 7.4, as measured using a voltohmmeter, are showed in (Fig. 4). TEER values showed an initial rapid exponential increase before a peak is reached at a value of about 1200 O.cm^2 (Ω.cm^2) (1 day) followed by a steep decline (2 days), and then a period where the TEER values of about

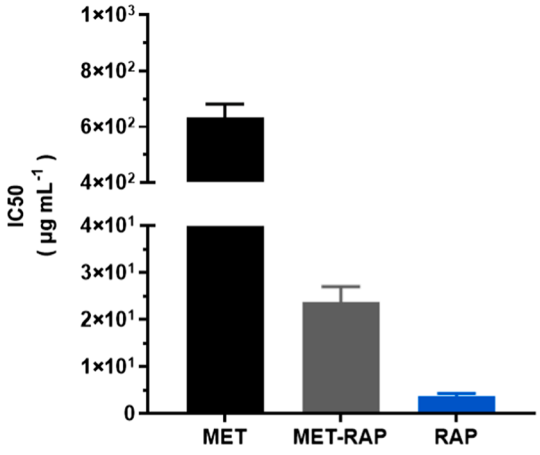

Fig. 3. 50% inhibitory concentration of the MET, MET-RAP formulation, and RAP on SIRC cell line. The IC50 was expressed as mean ± SEM from three independent experiments. MET IC50 = 632.9 ± 48.9 μg/mL, MET-RAP IC50 = 23.69 ± 2.76 μg/mL, RAP IC50 = 3.77 ± 0.59 μg/mL.

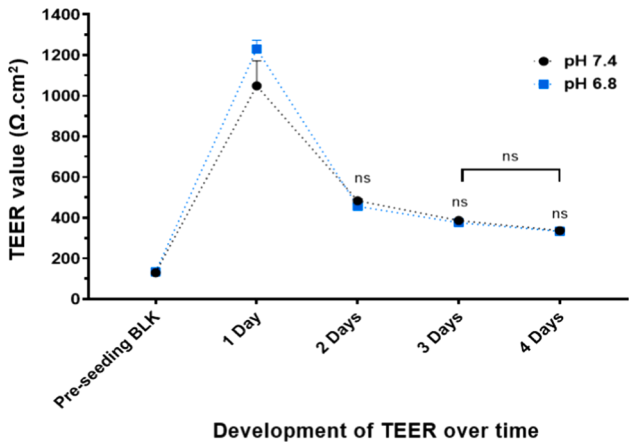

Fig. 4. The development of TEER for MDCK cells monolayer on transwells. The MDCK cells were grown over five days. There were no significant differences in the measured TEER values between pH 6.8 and 7.4 from day four. Statistical significance was determined by two-way ANOVA with Tukey's multiple comparison test t, n = 3.

300 Ω.cm^2 are stable (3–4 days). The TEER values increased during the exponential phase, with the steep increase in TEER corresponding to the growth and multiplication of cells before the cell monolayer reached confluence. This is followed by a subsequent drop in TEER due to tight junction formation. The TEER values were then stabilized in the stationary growth phase. Reaching a stable value of TEER is regarded as an indication of full differentiation of the epithelial monolayer with the formation of tight junctions in MDCK cells. There were no statistically significant differences in the measured TEER values between pH = 6.8 and 7.4 on day four. Thus, the subsequent transport assays were carried out during the periods of stable TEER values, i.e., Day 4–5 for the MDCK cell line at pH = 6.8 and 7.4.

A standard curve of FD-4 was freshly prepared with each replicate of the experiment. The standard curve plotted shows linearity over a concentration range of 0.977–125 μg/mL, with a correlation coefficient of 0.999. The equation of the standard curve (y = 244.34x + 12.585) was used to determine the concentration of the transported paracellular marker FD-4.

Fig. 5 shows the effect of the MET structure on transport across epithelial barriers in MDCK cells monolayer at pH 6.8 and 7.4 as measured using the paracellular marker FD-4. MET (DQ18%, DP20%) showed a significantly different permeability value at pH = 6.8 (Papp = $1.40 \times 10^{-5} \pm 2.25 \times 10^{-6}$ cm/s) compared to pH = 7.4 (Papp = $1.08 \times 10^{-5} \pm 3.83 \times 10^{-6}$ cm/s). MET is a weak base with a pKa of 6.0 (Lalatsa et al., 2012); this means that MET is less protonated at pH 7.4 than pH 6.8. Therefore, at a pH closer to pH = 6, MET is likely to enhance the paracellular transport compared to the physiological range. MET is an amphiphilic polymer that has a quaternary ammonium group. Quaternary amine polymers have been reported to open tight junctions at intestinal pH (Chen et al., 2013). The tight junction opening depends on

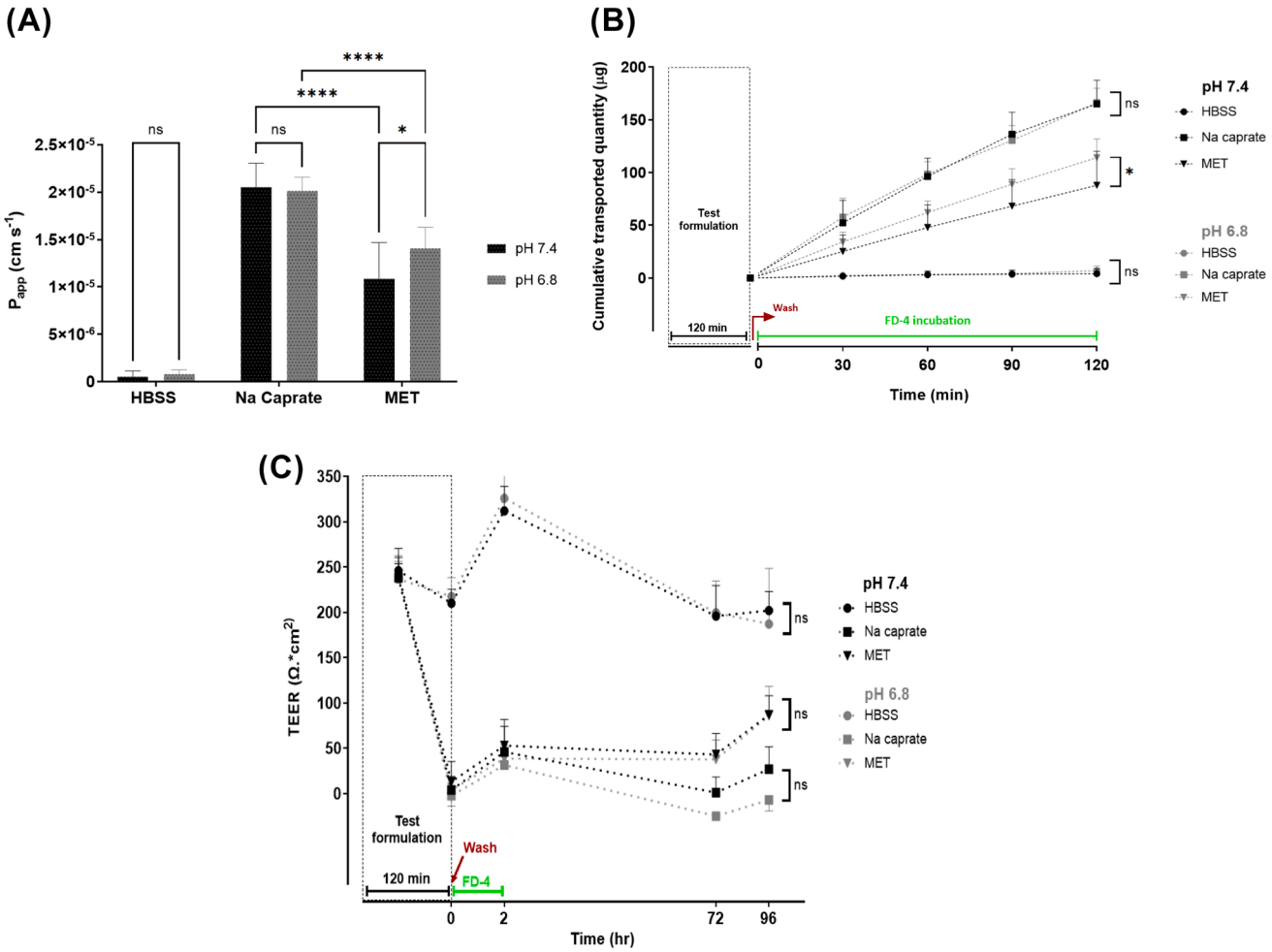

Fig. 5. Effect of MET on the paracellular transport of FD-4 across MDCK cell monolayer (pH: 6.8, 7.4). **(A)** Apparent permeability coefficient Papp at pH = 6.8 and 7.4; **(B)** Transport of FD-4 at pH = 6.8 and 7.4; **(C)** TEER value at pH = 6.8 and 7.4. MET was prepared at 1 mg/mL, and sodium caprate was prepared at 10 mM. Statistical data analysis was performed with two-way ANOVA followed by Tukey's multiple comparison test. The value $p < 0.05$ was considered significant, n = 3.

the degree of quaternization, meaning with a high degree of quaternization, the polymer will be more likely to have a higher charge density and be more likely to open tight junctions with the net result that such polymers with high levels of quaternary ammonium groups have a high solute transport capability (Chen et al., 2013). The MET Papp value at pH = 7.4 is statistically significant compared to the negative control HBSS at physiological pH. This means that MET could enhance tight junction opening and thus the paracellular transport at the tear pH, but to a lesser extent than it would at intestinal pH. These results were supported with the results from (Fig. 5B) in which the cumulative quantity of the transported FD-4 was significant at pH 6.8 compared to pH 7.4 due to the effect of the MET. However, there was no significant difference in the TEER value (Fig. 5C) between pH = 6.8 and 7.4, 96 h after treatment, meaning that the cells fully recovered after the treatment was removed.

MDCK cells differentiate into a columnar epithelium when grown on a suitable membrane and form tight junctions (Cho et al., 1989). They are considered a good model for the study of mammalian epithelia (Rothen-Rutishauser et al., 1998). The MDCK cell line has been used to study the functional nature and P-glycoprotein role in lowering the bioavailability of ocular topical drugs (Dey et al., 2004). Dey et al. reported the existence of the P-gp efflux pump in rabbit cornea and suggested that the efflux pump may be responsible for the low ocular bioavailability (Dey et al., 2004). Thus, the MDCK cell line was used as a well-known transport model that forms tight junctions. In these studies, we used the MDCK cell line to predict the transport across epithelia that presumably involves opening tight junctions and to predict the transport across epithelia where the P-glycoprotein efflux pump may be operational.

3.5. Biological in vivo studies

3.5.1. Pharmacokinetics study

3.5.1.1. Bioanalytical LC-MS/MS assay. The LC-MS/MS chromatograms for RAP and ascomycin are presented in (Supplementary Information, Fig. S1). Both RAP and ascomycin were ionized under the positive electrospray ionization for analyte quantification. The sodium adduct is employed as it was stable in the non-ammoniated mobile phase. Multiple reaction monitoring mode was utilized to detect RAP and ascomycin. The precursor ion to product ion transitions of *m/z* [M + Na]+ (936.4 → 409.1) and [M + Na] + *m/z* (814.2 → 604.1) were chosen for RAP and ascomycin, respectively, based on the most abundant product ion. The assay conditions had an adequate specificity for RAP, while no interfering peaks were observed at its retention time. The retention time was 3.44 and 3.30 min for RAP and ascomycin, respectively (Supplementary Information).

3.5.1.2. Preparation of standard and quality control curves. Working standards solutions were prepared to obtain a standard curve of RAP in the mobile phase and each of the tissues: cornea, conjunctiva, sclera, choroid-retina, aqueous humor, and vitreous humor. Table 3 shows the assay parameters used to analyze the tissues. Individual calibration curves for RAP in the mobile phase and each tissue were obtained by plotting the peak area ratios (RAP/ internal standard) versus the analyte concentration. The calibration curves were linear for RAP in a concentration range of 0.5–500 ng/mL for RAP in the mobile phase, with an r^2>0.99. The measured lower limit of quantification (LLOQ) for RAP was 0.5 ng/mL for RAP in the mobile phase and in the choroid-retina. The measured LLOQ for RAP in the cornea, aqueous humor, and vitreous humor was 1 ng/mL, while the measured LLOQ for RAP in the conjunctiva and the sclera was 10 ng/mL. The signal-to-noise ratios calculated by MassHunter workstation software were ≥ ten for the drug in the mobile phase and the drug in all tissues at the lower limit of quantification.

Table 3
Assay parameters of RAP in blank and ocular tissues.

Parameters	Equation of the straight line	Linearity (ng/mL)	r^2	Accuracy (%)	Precision (%)
Blank	y = 0.0607x + 0.3745	0.5–500	0.9972	–	–
Conjunctiva	y = 0.04x + 0.5204	10–500	0.9973	70.94	16.79
Aqueous humor	y = 0.0612x + 0.8589	1–500	0.9965	101.73	26.68
Vitreous humor	y = 0.0551x + 1.2327	1–500	0.9933	107.47	28.00
Cornea	y = 0.0619x + 0.7489	1–250	0.9920	105.97	27.61
Choroid-Retina	y = 0.0689x + 0.1223	0.5–500	0.9984	107.30	18.20
Sclera	y = 0.0345x + 0.1643	10–500	0.9988	52.42	11.10
Average				90.97	21.40
SD				23.52	7.03

Accuracy was examined by analyzing the RAP in the ocular tissues and RAP dissolved in the mobile phase. Accuracy was calculated by dividing the ratio of the peak area in the presence of the matrix to the peak area in the absence of a matrix multiplied by 100 (Guideline on bioanalytical method validation, 2012). The accuracy of the method must be between 85% and 115% of the nominal value in all the standards, except at the LLOQ level, which is between 80 and 120% according to bioanalytical method validation in the US Food and Drug Administration (US FDA) guidelines (Earla et al., 2012; Bioanalytical Method Validation Guidance for Industry, 2018). The average percentage of the accuracy of all the standards was 90.97%. This is in line with the guideline on bioanalytical method validation in which a range of ± 15% of the nominal value is acceptable for the non-zero calibrators and between ± 20% at the LLOQ. Precision was calculated using the coefficient of variation (CV) (standard deviation/mean) multiplied by 100. The precision of the method should be within 15% of the nominal concentration except at the LLOQ, which should be within 20% of the nominal concentration (Guideline on bioanalytical method validation, 2012). The average CV of all the standards was 21.40%. The average precision for the aqueous humor, vitreous humor and cornea fell outside these values, but accuracy for all the values within these tissues outside of the LLOQ ranged from 42.58 to 138.62%. The average precision in the main tissue of interest – the choroid retina - was 18.2%, with accuracy for all values outside of the LLOQ ranging from 74.24 to 127.17%.

3.5.1.3. MET-RAP pharmacokinetics animal study. We examined the delivery to the back of the eye using MET-RAP (25 μL, 0.2% w/v). The ocular tissue distribution study was conducted in healthy New Zealand White rabbits following topical instillation of the formulation into the conjunctival cul-de-sac. Topical single instillation of 0.2% w/v MET-RAP resulted in detectable and quantifiable RAP levels in the back of the eye tissues, i.e., sclera (total back and front) and choroid-retina. RAP concentrations were also quantified in the anterior chamber eye tissues, cornea, and conjunctiva. No RAP was detected in the aqueous humor and vitreous humor (LLOQ = 1 ng/mL) at all time points.

Fig. 6 shows the ocular drug distribution of RAP in a healthy rabbit model, and the pharmacokinetic parameters are presented in (Table 4). The Cmax of RAP in the sclera and the choroid-retina was 37 ± 47 ng/g (tmax = 2 h) and 145 ± 49 ng/g (tmax = 1 h), respectively. The Cmax of RAP in the cornea and the conjunctiva was 735 ± 339 ng/g (tmax = 1 h)

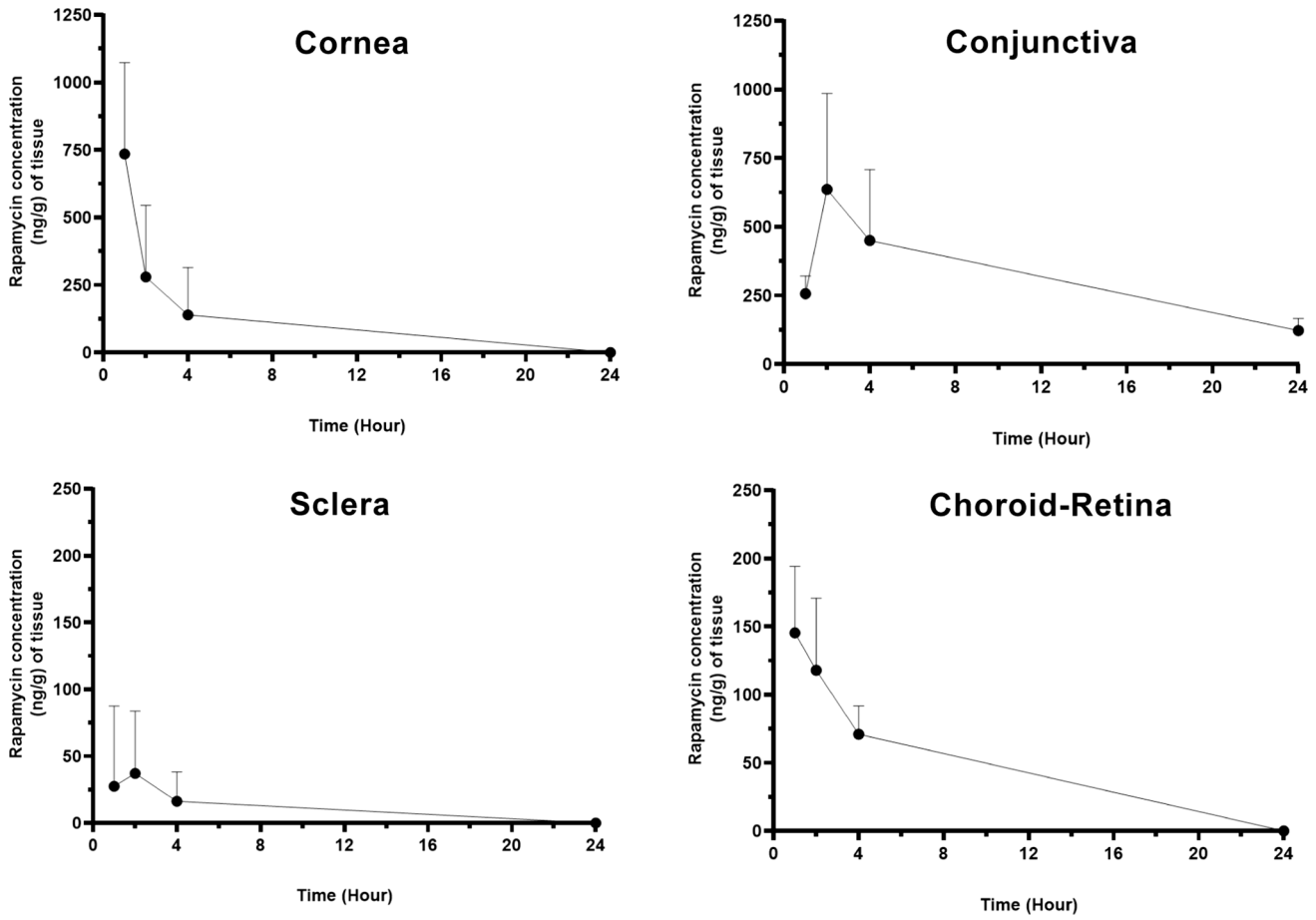

Fig. 6. *In vivo* RAP drug distribution in rabbit ocular tissues following the instillation of 25 μL of MET-RAP 0.2% w/v.

Table 4
Pharmacokinetics parameters of RAP after single ocular instillation of MET-RAP ophthalmic formulation solution in rabbits.

Pharmacokinetic parameters	Cornea	Conjunctiva	Sclera	Choroid-Retina
C_{max} (ng/g tissue)	735 ± 339	636 ± 349	37 ± 47	145 ± 49
T_{max} (hr)	1	2	2	1
AUC_{0-24} (ng.hr/g)	2691	7387	262	1103

and 636 ± 349 ng/g of tissue (tmax = 2 h), respectively. These tissue levels were achieved following a single ocular dose of 50 μg RAP in the MET-RAP formulation. High RAP drug concentrations were detected in the cornea and conjunctiva 1-hour post-dosing. The level of RAP in the cornea was 735 ± 339 ng/g of tissue and in the conjunctiva was 256 ± 65 ng/g of tissue.

A recent study reported RAP levels in the sclera and choroid-retina following the single-dose topical application of a nanomicellar eye drop formulation composed of vitamin E tocopherol polyethylene glycol succinate and octoxynol-40. RAP concentration in the sclera and choroid-retina was 486 ± 90 and 362 ± 56 ng/g of tissue, respectively (Cholkar et al., 2015). No RAP was detected in the vitreous humor (Cholkar et al., 2015). The level of RAP in the choroid-retina in the study was 2-fold the concentration identified in our study. The volume used by Cholkar et al. (Cholkar et al., 2015) was higher than the current work, 50 μL vs. 25 μL, which doubled the dose applied to 100 μg in the Cholkar study vs. 50 μg of RAP in the current study. When relating the level detected in the sclera to the total dose applied, about ~ 0.1% RAP of the total dose applied was detected in the sclera in our work compared to ~ 0.5% RAP in Cholkar et al. work. In another study, Earla et al. have reported the level of RAP in the cornea (2261 ± 507 ng/g tissue) after 1 h following a 50 μL administration of vitamin E tocopherol polyethylene glycol succinate: octoxynol-40: RAP formulation at a RAP concentration of 0.2% w/v (Earla et al., 2012). The level of RAP in the aqueous humor was below their reported limit of quantification (Earla et al., 2012). The level of RAP in the cornea in the Earla et al. (2.3% of the total dose applied) study was 50% higher than the level detected in the current work (1.5% of the total dose applied). This slight difference in tissue deposition levels may be due to the different volumes used in both studies. It is important to acknowledge that all animals in the previous two studies (Cholkar et al., 2015; Earla et al., 2012) were anesthetized before the dosing, and the anesthesia was maintained throughout the experiment. There is growing evidence that gravity markedly influences vertical eye position and movement (Pierrot-Deseilligny, 2009). Arguably, when the eyelids are closed and the animals in a horizontal position, there will be an absence of gravity associated with preventing rapid drainage of applied eyedrops through the nasolacrimal duct. Our work was conducted on awake rabbits, and the blink rate was recorded. It is our view that the differences in drug levels seen in these earlier studies when compared to our own may be attributed to the different study designs (anesthetized rabbits in the earlier studies vs. awake rabbits in the current study). The average tear fluid volume is approximately 7 μL in both rabbits and humans (Ham et al., 2006). It has been reported that the tear turnover rate in non-anesthetized rabbits is about 0.53 μL/min, with a range of 0.47–0.66 μL/min. In anesthetized animals, tear turnover rate is negligibly small or absent (Chrai et al., 1973). The tear turnover in awake animals would impact on the residence time of the formulation in the corneal pocket and could reduce drug absorption compared to anesthetized rabbits. Our results confirm previous findings

(Cholkar et al., 2015) on the absence of RAP in the vitreous humor.

For a topical drug to reach the back of the eye tissue, it may follow the corneal and/or conjunctival-scleral pathway (Hughes et al., 2005). RAP is practically insoluble in water, and due to its high lipophilicity, the drug was not able to translocate across the cornea to the aqueous humor and vitreous humor. Since the drug must cross the corneal barrier to reach the aqueous humor and retina (Cochereau-Massin et al., 1991), this indicates that RAP may follow the conjunctival/ scleral pathway to arrive at the retina. We have shown that MET, with its mucoadhesive properties (Siew et al., 2012), acts as a permeation enhancer, enabling RAP to come in close proximity to the cells and permeate the tissues, and to deliver the drug to the choroid-retina in a concentration higher than its therapeutic levels (7–12 ng/mL) (Buech et al., 2007). The purpose of the study was to use a needle-free formulation to achieve a therapeutic effect. These results indicate that MET may be used as a novel carrier for RAP, and the formulation could be an alternative to the current invasive injections/ implant approaches used to access the retina.

3.5.1.4. Ocular tolerability. The blink rate following dosing is an acceptable method of assessing acute ocular irritation (Carlisle and Digiovanni, 2015), although other parameters such as erythema and swelling are also used to assess ocular irritation. The blink rate was assessed in the first 60 s post-dosing after a single instillation of MET-RAP (25 μL, 0.2% w/v). The number of blinks was taken as a preliminary investigation into the possible irritant nature of the formulation. Normal saline (25 μL) was used as a control ($n = 6$ eyes). The average blink rate in both eyes in the normal saline group was recorded as 1.0 ± 0.41 blinks/min. The average blink rate in both eyes in all treatment groups was reported as (5.10 ± 0.52 blinks/min, $p > 0.05$) (Fig. 7A). Rabbits share ocular features with humans, including a comparable vitreous volume and internal structure, and thus a similar diffusional path for topically administered compounds to reach the posterior segment (Rodrigues et al., 2018). The rabbits blink at a rate of 4–5 blinks/60 min (Rodrigues et al., 2018) when compared to the human blink rate (17.6 ± 2.4 blinks/min during rest) (Bentivoglio et al., 1997; Kaminer et al., 2011). This may suggest that there is a difference in the reaction to drugs between rabbits and humans because rabbits seem to show higher ocular sensitivity to instilled substances (Toshida et al., 2009), and there may be a more considerable contact time for drugs topically applied in the animal due to its significantly lower blink rate (Maurice, 1995). It is noteworthy that a direct comparison to a standard irritant substance such as RAP alone or high concentrations of sodium lauryl sulfate (Bondi et al., 2015) has not been carried out.

The assessment of irritation of the MET-RAP formulation to rabbits' eyes was visually evaluated using the criteria of erythema and swelling (Fig. 7B). There were no visible signs of erythema, tearing or swelling, following the ocular administration of MET-RAP. These data suggested that MET-RAP as a formulation, while increasing the rabbit eye blink rate, does not cause dose-limiting ocular irritation to rabbits' eyes, and it is a capable system for topical treatment of inflammatory retinal diseases.

3.5.2. MET-RAP animal pharmacodynamic study in C57BL/6J mice

Experimental autoimmune uveitis is being used as a model of retinal disease. In this study, this animal model was used to explore the impact of an aqueous-based lipophilic drug-loaded polymeric nanoparticle formulation (MET-RAP) intended for topical ocular delivery to treat inflammatory/autoimmune ocular mouse disease and to investigate the mechanism of action of RAP in the EAU model.

3.5.2.1. EAU clinical scoring. All animals in all groups showed early signs of the development of EAU at day 13 (pre-treatment, Fig. 8A). The average scores of the negative control groups were (2.90 ± 0.88 and 3.80 ± 0.79) for the saline and MET groups pre-treatment, respectively. The average score of the positive control group DEX was (4.00 ± 0.94), while the treatment group MET-RAP scored (3.50 ± 0.94). There were no statistically significant differences ($p > 0.05$) among all groups on day 13 (pre-treatment).

The clinical scoring post-treatment (day 20, 7 days of treatment) are shown in (Fig. 8B). The average scores of the negative control groups were (10.70 ± 4.88 and 13.60 ± 3.81) for the saline and MET groups post-treatment, respectively. There were no statistically significant differences ($p > 0.05$) among the negative control groups at day 20 (post-treatment), suggesting a severe progression of the EAU and no effect of the negative control treatments on suppressing EAU development. The treatment group MET-RAP showed a statistically significant difference ($p < 0.05$) compared to the negative control groups. The average score of all animals in the formulation MET-RAP group post-treatment was (4.80 ± 2.30). Also, the positive control group DEX scored (6.50 ± 1.90) on day 20. Despite a lower scoring of the MET-RAP formulation when

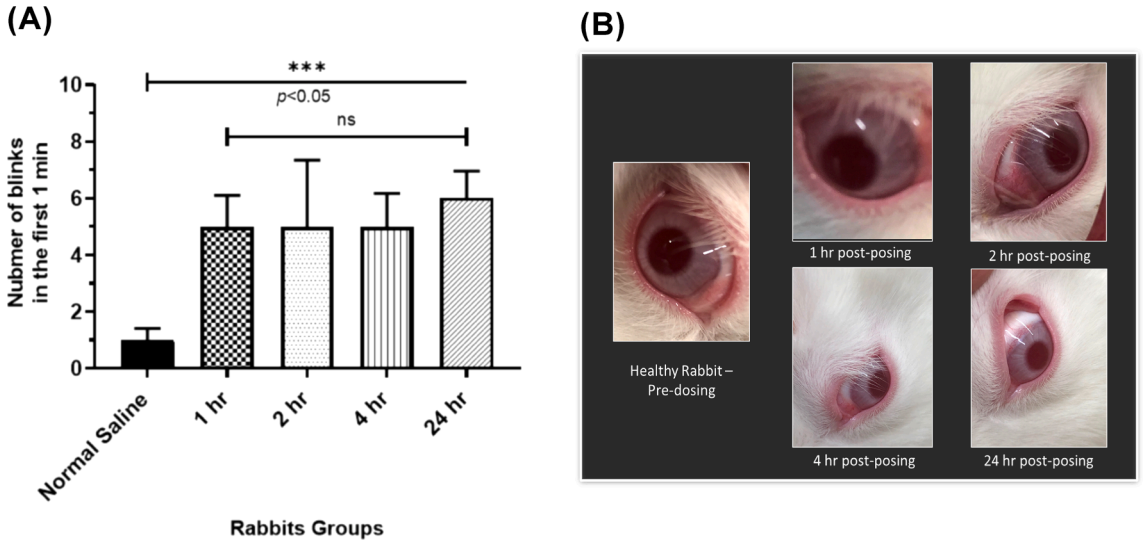

Fig. 7. Assessment of ocular tolerability of the MET-RAP formulation to rabbits' eyes. **(A)** The average blink rate in both eyes, assessed immediately after dosing in all treatment groups (animals killed at 1 hr, 2 hr, 4 hr and 24 hr) = 5.10 ± 0.52 blinks/min compared to negative control group = 1.0 ± 0.41 blinks/min ($p < 0.05$). **(B)** All rabbits showed no signs of erythema, tearing or swelling, following the ocular administration of MET-RAP formulation – animals were examined immediately after dosing. Statistical analysis was performed on the blink rate with One-way ANOVA with Tukey's multiple comparison analysis. The value $p < 0.05$ was considered significant.

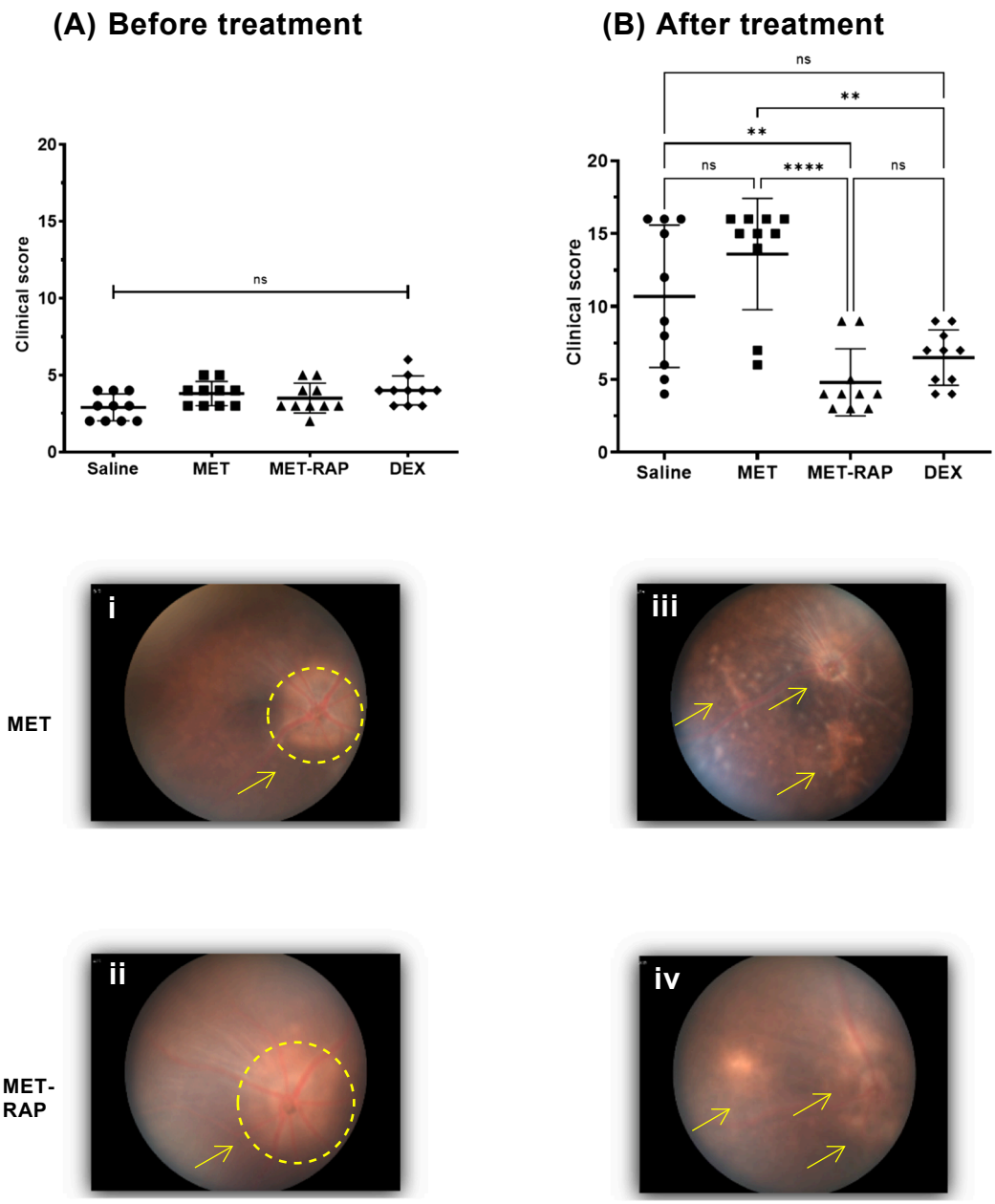

Fig. 8. Clinical scoring and fundoscopy images of the EAU experiment. **(A)** at day 13 (pre-treatment), **(B)** at day 20, (post-treatment). Fundus images from an IRBP-immunized mouse show EAU development pre-treatment in **(i)** MET control groups, **(ii)** MET-RAP formulation group. Fundus images post-treatment showing severe EAU in **(iii)** MET control groups. **(iv)** MET-RAP formulation after treatment group showing no signs of progression of EAU. Arrows indicate areas of interest.

compared to the DEX group, there were no statistically significant differences ($p > 0.05$) between the MET-RAP group and the positive control group (DEX) on day 20 (post-treatment). Additionally because of the variable response to saline post treatment, there was no statistical significance between the DEX group and saline ($p > 0.05$). These results suggest that MET-RAP formulation was able to suppress EAU progression, and it was as effective as marketed eye drops Maxidex®.

Fundoscopy data from the EAU experiment imaged are shown in Fig. 8. Before the treatment, both groups (MET and MET-RAP) showed clear evidence of early disease development with inflammation around the optic nerve. The representative fundus images from an IRBP-immunized mouse treated with the MET control showed severe EAU on day 20, while a substantial attenuation of clinical signs following topical treatment with the MET-RAP formulation was observed at the end of the experiment, on day 20.

3.5.2.2. Retinal immunophenotyping by flow cytometry. Immunophenotyping of retinal cells isolated from enucleated eyes post-treatment, using flow cytometry, is presented in this section. Retinal flow cytometry identified the presence of $CD4^+$ T cells in all treatment groups with no significant differences (Supplementary Information, Fig. S2). However, a statistically significant decrease was observed in the total RORγt level in $CD4^+$ T cells treated with MET-RAP compared to the negative control and the positive control (Fig. 9A). RORγt is a specifying transcription factor of Th17, which belongs to the RAR-related orphan nuclear receptor family and regulates Th17-associated genes such as IL-17 and Th17 differentiation (Castro et al., 2017). Th17 cells play an essential role in the development of autoimmune diseases. The cytokines involved in Th17-mediated autoimmune diseases are important contributors to the pathogenic changes observed in EAU (Sun et al., 2015). There were no statistically significant differences in the expression level of IL-17 between all treatment groups.

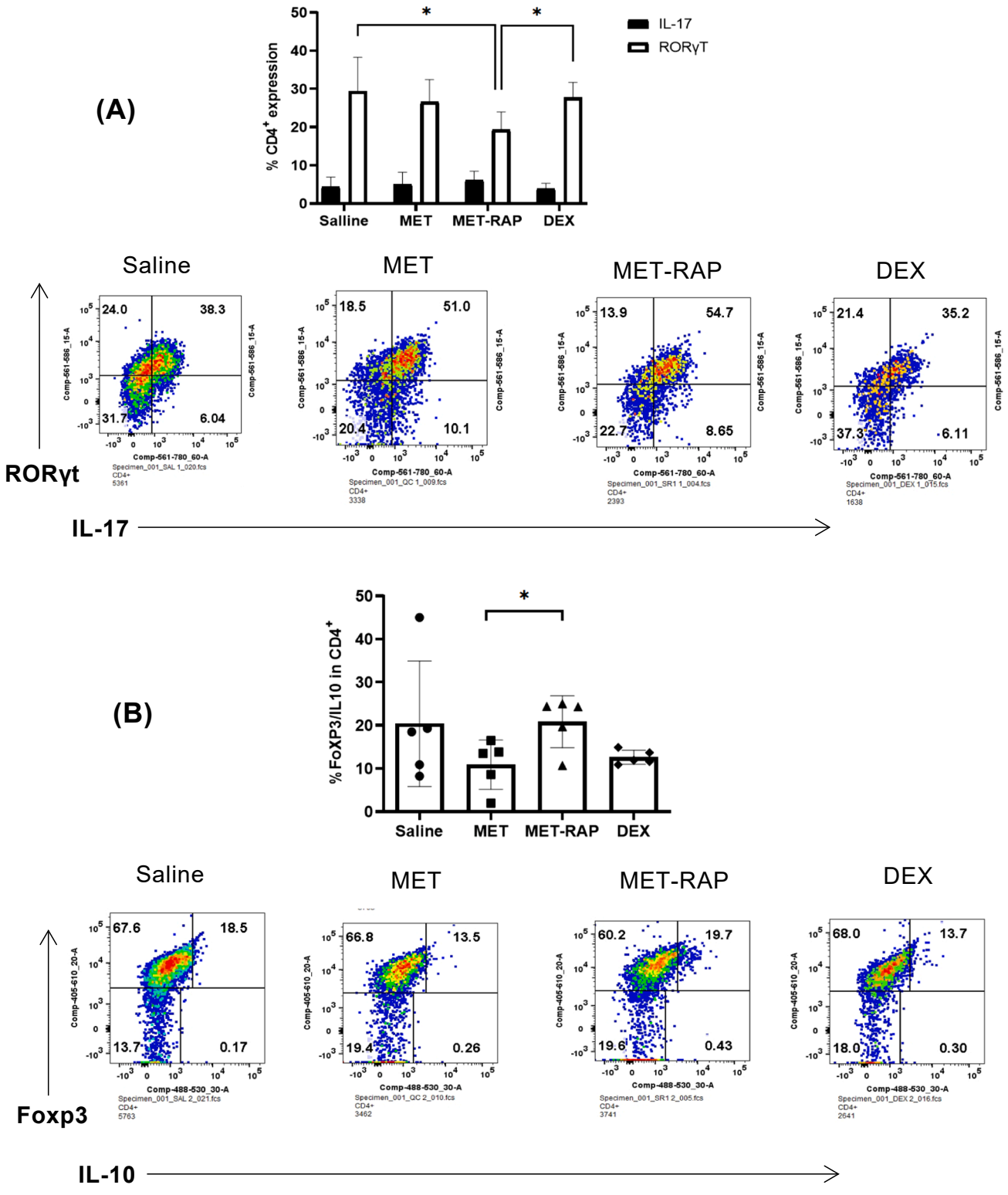

Fig. 9. Flow cytometer plot of the expression of (A) IL-17 and RORγt in $CD4^+$ T cell; (B) Foxp3 and IL-10 in $CD4^+$ T cell.

The T-box transcription factor is expressed in $CD4^+$ T lymphocytes and committed to Th1 T-cell development (Dorfman et al., 2005). We found no significant differences in the expression of both RORγt and T-bet for the MET-RAP formulation compared to other groups (Supplementary Information, Fig. S3). Double positive $ROR\gamma t^+/T\text{-}bet^+$ cells have been reported in EAU (Shoda et al., 2015), but their uveitogenicity remains to be investigated. This could suggest that MET-RAP does not affect Th1/17 or Th1 cells in EAU progression compared to controls. Unfortunately, we did not obtain reliable data on the IFNγ expression as a cytokine marker for Th1 cells to conclude on the impact of MET-RAP on Th1 cells. However, we have shown here that MET-RAP formulation specifically attenuates EAU progression by lowering the RORγt expression (Fig. 9A).

The Foxp3 is a lineage specifying transcription factor for T regulatory

cells within the $CD4^+CD25^+$ T cell population (Liu et al., 2013; Lu et al., 2014). Fig. 9B showed the increased expression of Foxp3 and IL-10 in the MET-RAP treated group compared to the vehicle control. These results suggested that the specificity of MET-RAP formulation on attenuating EAU progression through increasing Treg cells level.

In the present study, we explored the impact of a MET-RAP novel formulation on delivering RAP to the back of the eye upon topical application of eye drops and in a separate study the effect of MET-RAP on EAU. We have shown that MET-RAP decreased the RORγt level, increased Foxp3 expression and IL-10 secretion, and suppressed the disease progression. These results suggest that MET-RAP may switch $CD4^+$ T cell polarity from a Th17 to Treg phenotype, and thus represents a possible therapeutic point for a wide range of inflammatory and autoimmune disorders, including posterior uveitis.

4. Conclusion

The corneal epithelial mucosa possesses an overall negative charge. Thus, the adhesion of positively charged nanoparticles such as MET is favored at physiological pH. We show that MET is a permeation enhancer, and this is supported by detecting sufficient drugs in the ocular tissues within our awake rabbit model. The MET-RAP formulation was stable for 28 days at room temperature and on refrigeration. MET delivered RAP into the rabbits' ocular tissues and delivered the drug to the choroid-retina in a concentration higher than RAP therapeutic levels. MET-RAP successfully controlled the progression of EAU in a mouse model of EAU. We have shown that MET-RAP decreased the level of RORγt, increased Foxp3 expression, and IL-10 secretion, and thus conclude that it is likely that RAP is able to reduce the progression of EAU via a polarity switch between Th17 and Treg CD4 + T-cells. MET-RAP eye drops could thus be used to control a wide range of inflammatory and autoimmune disorders, including posterior uveitis.

Declaration of Competing Interest

The authors declare the following financial interests/personal relationships which may be considered as potential competing interests: Ijeoma F. Uchegbu reports equipment, drugs, or supplies was provided by Nanomerics Ltd. Ijeoma F. Uchebgu reports a relationship with Nanomerics Ltd that includes: equity or stocks. Ijeoma F. Uchegbu has patent pending to Nanomerics Ltd. UCL. Ijeoma F. Uchegbu and Andreas G. Schatzlein are Nanomerics directors.

Acknowledgments

The authors would like to thank Nanomerics Ltd. for supplying the polymer excipients. We also thank the Umm AlQura University (Kingdom of Saudi Arabia) for providing a scholarship to MYB.

Funding

This research did not receive any specific grant from funding agencies in the public, commercial, or not-for-profit sectors.

Appendix A. Supplementary data

Supplementary data to this article can be found online at https://doi.org/10.1016/j.ijpharm.2022.121755.

References

Agarwal, R.K., Caspi, R.R., 2012. Rodent models of experimental autoimmune uveitis. Methods Mol. Med. 900, 443–469. https://doi.org/10.1007/978-1-60761-720-4_22.

Ahmad, S., Johnston, B.F., Mackay, S.P., Schatzlein, A.G., Gellert, P., Sengupta, D., Uchegbu, I.F., 2010. In silico modelling of drug-polymer interactions for pharmaceutical formulations. J. R. Soc. Interface. 7 (suppl_4) https://doi.org/10.1098/rsif.2010.0190.focus.

Badr, M.Y., Abdulrahman, N.S., Schatzlein, A.G., Uchegbu, I.F., 2021. A polymeric aqueous tacrolimus formulation for topical ocular delivery. Int. J. Pharm. 599, 120364. https://doi.org/10.1016/j.ijpharm.2021.120364.

Baranowski, P., Karolewicz, B., Gajda, M., Pluta, J., 2014. Ophthalmic drug dosage forms: Characterisation and research methods. Sci. World J. 2014, 1–14. https://doi.org/10.1155/2014/861904.

Bentivoglio, A.R., Bressman, S.B., Cassetta, E., Carretta, D., Tonali, P., Albanese, A., 1997. Analysis of blink rate patterns in normal subjects. Mov. Disord. 12 (6), 1028–1034. https://doi.org/10.1002/mds.870120629.

Bioanalytical Method Validation Guidance for Industry, 2018. http://www.fda.gov/Drugs/GuidanceComplianceRegulatoryInformation/Guidances/default.htmand/orhttp://www.fda.gov/AnimalVeterinary/GuidanceComplianceEnforcement/GuidanceforIndustry/default.htm (accessed November 29, 2020).

Boldison, J., Chu, C.J., Copland, D.A., Lait, P.J.P., Khera, T.K., Dick, A.D., Nicholson, L. B., 2014. Tissue-Resident Exhausted Effector Memory CD8 + T Cells Accumulate in the Retina during Chronic Experimental Autoimmune Uveoretinitis. J. Immunol. 192 (10), 4541–4550. https://doi.org/10.4049/jimmunol.1301390.

Bondi, C.A.M., Marks, J.L., Wroblewski, L.B., Raatikainen, H.S., Lenox, S.R., Gebhardt, K. E., 2015. Human and Environmental Toxicity of Sodium Lauryl Sulfate (SLS): Evidence for Safe Use in Household Cleaning Products. Environ. Health Insights. 9, 27–32. https://doi.org/10.4137/EHI.S31765.

Buech, G., Bertelmann, E., Pleyer, U., Siebenbrodt, I., Borchert, H.-H., 2007. Formulation of sirolimus eye drops and corneal permeation studies. J. Ocul. Pharmacol. Ther. 23 (3), 292–303. https://doi.org/10.1089/jop.2006.130.

Carlisle, R.T., Digiovanni, J., 2015. Differential diagnosis of the swollen red eyelid. Am. Fam. Physician. 92, 106–112.

Caspi, R.R., 2003. Experimental Autoimmune Uveoretinitis in the Rat and Mouse. Curr. Protoc. Immunol. 53 (1) https://doi.org/10.1002/0471142735.im1506s53.

Castro, G., Liu, X., Ngo, K., De Leon-Tabaldo, A., Zhao, S., Luna-Roman, R., Yu, J., Cao, T., Kuhn, R., Wilkinson, P., Herman, K., Nelen, M.I., Blevitt, J., Xue, X., Fourie, A., Fung-Leung, W.-P., Chung, Y., 2017. RORγt and RORα signature genes in human Th17 cells. PLoS ONE 12 (8), e0181868. https://doi.org/10.1371/journal.pone.0181868.

Chen, M.-C., Mi, F.-L., Liao, Z.-X., Hsiao, C.-W., Sonaje, K., Chung, M.-F., Hsu, L.-W., Sung, H.-W., 2013. Recent advances in chitosan-based nanoparticles for oral delivery of macromolecules. Adv. Drug Deliv. Rev. 65 (6), 865–879. https://doi.org/10.1016/j.addr.2012.10.010.

Cho, Y., Ha, E.S., Baek, I.H., Kim, M.S., Cho, C.W., Hwang, S.J., 2015. Enhanced supersaturation and oral absorption of sirolimus using an amorphous solid dispersion based on Eudragit® E. Molecules 20, 9496–9509. https://doi.org/10.3390/molecules20069496.

Cho, M.J., Thompson, D.P., Cramer, C.T., Vidmar, T.J., Scieszka, J.F., 1989. The Madin Darby Canine Kidney (MDCK) Epithelial Cell Monolayer as a Model Cellular Transport Barrier. Pharm. Res. An Off. J. Am. Assoc. Pharm. Sci. 6, 71–77. https://doi.org/10.1023/A:1015807904558.

Cholkar, K., Gunda, S., Earla, R., Pal, D., Mitra, A.K., 2015. Nanomicellar Topical Aqueous Drop Formulation of Rapamycin for Back-of-the-Eye Delivery. AAPS PharmSciTech. 16 (3), 610–622. https://doi.org/10.1208/s12249-014-0244-2.

Chooi, K.W., Simão Carlos, M.I., Soundararajan, R., Gaisford, S., Arifin, N., Schätzlein, A. G., Uchegbu, I.F., 2014. Physical characterisation and long-term stability studies on quaternary ammonium palmitoyl glycol chitosan (GCPQ) - A new drug delivery polymer. J. Pharm. Sci. 103 (8), 2296–2306. https://doi.org/10.1002/jps.24026.

Chrai, S.S., Patton, T.F., Mehta, A., Robinson, J.R., 1973. Lacrimal and Instilled Fluid Dynamics in Rabbit Eyes. J. Pharm. Sci. 62 (7), 1112–1121. https://doi.org/10.1002/jps.2600620712.

Cochereau-Massin, I., Bauchet, J., Faurisson, F., Vallois, J.M., Lacombe, P., Pocidalo, J.J., 1991. Ocular kinetics of pefloxacin after intramuscular administration in albino and pigmented rabbits. Antimicrob. Agents Chemother. 35 (6), 1112–1115. https://doi.org/10.1128/AAC.35.6.1112.

Dey, S., Gunda, S., Mitra, A.K., 2004. Pharmacokinetics of Erythromycin in Rabbit Corneas after Single-Dose Infusion: Role of P-Glycoprotein as a Barrier to in Vivo Ocular Drug Absorption. J. Pharmacol. Exp. Ther. 311 (1), 246–255. https://doi.org/10.1124/jpet.104.069583.

Dick, A.D., 1995. Retinal antigen-specific t cells mediate experimental autoimmune uveoretinitis (EAU) in PVG rat a model for tracking antigen-specific CD4+ t cells in the inflamed Eye. Ocul. Immunol. Inflamm. 3 (4), 261–270. https://doi.org/10.3109/09273949509069120.

Dorfman, D.M., Hwang, E.S., Shahsafaei, A., Glimcher, L.H., 2005. T-bet, a T cell-associated transcription factor, is expressed in Hodgkin's lymphoma. Hum. Pathol. 36 (1), 10–15. https://doi.org/10.1016/j.humpath.2004.10.006.

Durrani, O.M., Tehrani, N.N., Marr, J.E., Moradi, P., Stavrou, P., Murray, P.I., 2004. Degree, duration, and causes of visual loss in uveitis. Br. J. Ophthalmol. 88, 1159–1162. https://doi.org/10.1136/bjo.2003.037226.

Dutcher, J.P., Motzer, R.J., Atkins, M.B., Figlin, R.A., Kaelin, W.G., Stadler, W.M., Gordon, M.S., George, D.J., 2004. Mammalian target of rapamycin inhibition. Clin. Cancer Res. https://doi.org/10.1158/1078-0432.CCR-050008.

Earla, R., Cholkar, K., Gunda, S., Earla, R., Mitra, A.K., 2012. Bioanalytical method validation of rapamycin in ocular matrix by QTRAP LC–MS/MS: Application to rabbit anterior tissue distribution by topical administration of rapamycin nanomicellar formulation. J. Chromatogr. B Anal. Technol. Biomed. Life Sci. 76–86. https://doi.org/10.1111/j.1743-6109.2008.01122.x.Endothelial.

Ensign, L.M., Duh, E.J., Ding, Z., Oh, Y., Hartsock, M.J., Xu, Q., Luo, L., Xia, S., Hanes, J., Yang, J., Stark, W.J., Meng, T., Thorne, J.E., Eberhart, C.G., Kim, Y.-C., 2019. Controlled release of corticosteroid with biodegradable nanoparticles for treating experimental autoimmune uveitis. J. Control. Release. 296, 68–80. https://doi.org/10.1016/j.jconrel.2019.01.018.

Eskandarpour, M., Alexander, R., Adamson, P., Calder, V.L., 2017. Pharmacological Inhibition of Bromodomain Proteins Suppresses Retinal Inflammatory Disease and Downregulates Retinal Th17 Cells. J. Immunol. 198 (3), 1093–1103. https://doi.org/10.4049/jimmunol.1600735.

Highlights of Prescribing Information, FDA. (2010). www.fda.gov/medwatch (accessed April 10, 2020).

FDA's acceptance of Santen's Opsiria marks a milestone for the company, (n.d.). https://www.pharmaceutical-technology.com/comment/commentfdas-acceptance-of-santens-opsiria-marks-a-milestone-for-the-company-5802460/ (accessed April 18, 2020).

Forrest, M.L., Won, C.-Y., Malick, A.W., Kwon, G.S., 2006. In vitro release of the mTOR inhibitor rapamycin from poly(ethylene glycol)-b-poly(ε-caprolactone) micelles. J. Control. Release. 110 (2), 370–377. https://doi.org/10.1016/j.jconrel.2005.10.008.

Gegg, M.E., Harry, R., Hankey, D., Zambarakji, H., Pryce, G., Baker, D., Adamson, P., Calder, V., Greenwood, J., 2005. Suppression of Autoimmune Retinal Disease by Lovastatin Does Not Require Th2 Cytokine Induction. J. Immunol. 174 (4), 2327–2335. https://doi.org/10.4049/jimmunol.174.4.2327.

Guideline on bioanalytical method validation, 44 (2012) 1–23.

Ham, B.M., Cole, R.B., Jacob, J.T., 2006. Identification and comparison of the polar phospholipids in normal and dry eye rabbit tears by MALDI-TOF mass spectrometry. Investig. Ophthalmol. Vis. Sci. 47, 3330–3338. https://doi.org/10.1167/iovs.05-0756.

Hancock, B.C., Parks, M., 2000. What is the True Solubility Advantage for Amorphous Pharmaceuticals? Pharm. Res. 17, 397–404. http://library1.nida.ac.th/termpaper6/sd/2554/19755.pdf.

Heaton, A., Ward, M.K., Johnston, D.G., Alberti, K.G., Kerr, D.N., 1986. Evaluation of glycerol as an osmotic agent for continuous ambulatory peritoneal dialysis in end-stage renal failure. Clin. Sci. (Lond) 70, 23–29. https://doi.org/10.1042/CS0700023.

Hughes, P., Olejnik, O., Changlin, J., Wilson, C., 2005. Topical and systemic drug delivery to the posterior segments. Adv. Drug Deliv. Rev. 57 (14), 2010–2032. https://doi.org/10.1016/j.addr.2005.09.004.

Iyamu, E., Enobakhare, O., 2019. pH and Osmolality of Pre-corneal Tear Film and Commercially Available Artificial Tears. EC Ophthalmol. 11, 17–25.

Kaminer, J., Powers, A.S., Horn, K.G., Hui, C., Evinger, C., 2011. Characterizing the spontaneous blink generator: An animal model. J. Neurosci. 31 (31), 11256–11267. https://doi.org/10.1523/JNEUROSCI.6218-10.2011.

Kim, M.S., Kim, J.S., Park, H.J., Cho, W.K., Cha, K.H., Hwang, S.J., 2011. Enhanced bioavailability of sirolimus via preparation of solid dispersion nanoparticles using a supercritical antisolvent process. Int. J. Nanomed. 6, 2997–3009. https://doi.org/10.2147/IJN.S26546.

Korson, L., Drost-Hansen, W., Millero, F.J., 1969. Viscosity of water at various temperatures. J. Phys. Chem. 73 (1), 34–39. https://doi.org/10.1021/j100721a006.

Krug, S.M., Amasheh, M., Dittmann, I., Christoffel, I., Fromm, M., Amasheh, S., 2013. Sodium caprate as an enhancer of macromolecule permeation across tricellular tight junctions of intestinal cells. Biomaterials 34 (1), 275–282. https://doi.org/10.1016/j.biomaterials.2012.09.051.

Lalatsa, A., Garrett, N.L., Ferrarelli, T., Moger, J., Schätzlein, A.G., Uchegbu, I.F., 2012. Delivery of peptides to the blood and brain after oral uptake of quaternary ammonium palmitoyl glycol chitosan nanoparticles. Mol. Pharm. 9 (6), 1764–1774. https://doi.org/10.1021/mp300068j.

Li, J., Kim, S., Blenis, J., 2014. Rapamycin: one drug, many effects. Cell Metab. 19 (3), 373–379. https://doi.org/10.1016/j.cmet.2014.01.001.

Liu, X., Gao, N.a., Li, M., Xu, D., Hou, Y., Wang, Q., Zhang, G., Sun, Q., Zhang, H., Zeng, X., Zheng, S.G., 2013. Elevated Levels of CD4+CD25+FoxP3+ T Cells in Systemic Sclerosis Patients Contribute to the Secretion of IL-17 and Immunosuppression Dysfunction. PLoS ONE 8 (6), e64531. https://doi.org/10.1371/journal.pone.0064531.

López-Dávila, V., Magdeldin, T., Welch, H., Dwek, M.V., Uchegbu, I., Loizidou, M., 2016. Efficacy of DOPE/DC-cholesterol liposomes and GCPQ micelles as AZD6244 nanocarriers in a 3D colorectal cancer in vitro model. Nanomedicine. 11 (4), 331–344. https://doi.org/10.2217/nnm.15.206.

Lu, Y., Wang, J., Gu, J., Lu, H., Li, X., Qian, X., Liu, X., Wang, X., Zhang, F., Lu, L., 2014. Rapamycin regulates iTreg function through CD39 and Runx1 pathways. J. Immunol. Res. 2014, 1–8. https://doi.org/10.1155/2014/989434.

Maurice, D., 1995. The effect of the low blink rate in rabbits on topical drug penetration. J. Ocul. Pharmacol. Ther. 11 (3), 297–304. https://doi.org/10.1089/jop.1995.11.297.

Milani, B.Y., Milani, F.Y., Park, D.-W., Namavari, A., Shah, J., Amirjamshidi, H., Ying, H., Djalilian, A.R., 2013. Rapamycin inhibits the production of myofibroblasts and reduces corneal scarring after photorefractive keratectomy. Investig. Ophthalmol. Vis. Sci. 54 (12), 7424. https://doi.org/10.1167/iovs.13-12674.

Nezlin, A., 2003. Handbook of modern pharmaceutical analysis. Handbook of modern pharmaceutical analysis 56 (3), 507–508.

Nguyen, Q.D., Merrill, P.T., Sepah, Y.J., Ibrahim, M.A., Banker, A., Leonardi, A., Chernock, M., Mudumba, S., Do, D.V., 2018. Intravitreal Sirolimus for the Treatment of Noninfectious Uveitis: Evolution through Preclinical and Clinical Studies. Ophthalmology 125 (12), 1984–1993. https://doi.org/10.1016/j.ophtha.2018.06.015.

Niazi, S., 2003. Stability Testing of New Drug Substances and Products, https://doi.org/10.3109/9781420081244-10.

Pierrot-Deseilligny, C., 2009. Effect of gravity on vertical eye position, in: Ann. N. Y. Acad. Sci., Blackwell Publishing Inc., pp. 155–165. https://doi.org/10.1111/j.1749-6632.2009.03864.x.

Powell, J.D., Delgoffe, G.M., 2010. The mammalian Target of Rapamycin (mTOR) provides a critical link between T cell differentiation, function and metabolism, https://doi.org/10.1016/j.immuni.2010.09.002.

Qu, X., Khutoryanskiy, V.V., Stewart, A., Rahman, S., Papahadjopoulos-Sternberg, B., Dufes, C., McCarthy, D., Wilson, C.G., Lyons, R., Carter, K.C., Schätzlein, A., Uchegbu, I.F., 2006. Carbohydrate-based micelle clusters which enhance hydrophobic drug bioavailability by up to 1 order of magnitute. Biomacromolecules 7, 3452–3459. https://doi.org/10.1021/bm0604000.

Rodrigues, G.A., Lutz, D., Shen, J., Yuan, X., Shen, H., Cunningham, J., Rivers, H.M., 2018. Topical Drug Delivery to the Posterior Segment of the Eye: Addressing the Challenge of Preclinical to Clinical Translation. Pharm. Res. 35 (12) https://doi.org/10.1007/s11095-018-2519-x.

Rothen-Rutishauser, B., Krämer, S.D., Braun, A., Günthert, M., Wunderli-Allenspach, H., 1998. MDCK cell cultures as an epithelial in vitro model: Cytoskeleton and tight junctions as indicators for the definition of age-related stages by confocal microscopy. Pharm. Res. 15, 964–971. https://doi.org/10.1023/A:1011953405272.

Serrano, D.R., Lalatsa, A., Dea-Ayuela, M.A., Bilbao-Ramos, P.E., Garrett, N.L., Moger, J., Guarro, J., Capilla, J., Ballesteros, M.P., Schätzlein, A.G., Bolás, F., Torrado, J.J., Uchegbu, I.F., 2015. Oral particle uptake and organ targeting drives the activity of amphotericin B nanoparticles. Mol. Pharm. 12 (2), 420–431. https://doi.org/10.1021/mp500527x.

Shanmuganathan, V.A., Casely, E.M., Raj, D., Powell, R.J., Joseph, A., Amoaku, W.M., Dua, H.S., 2005. The efficacy of sirolimus in the treatment of patients with refractory uveitis. Br. J. Ophthalmol. 89, 666–669. https://doi.org/10.1136/bjo.2004.048199.

Shoda, H., Yanai, R., Yoshimura, T., Nagai, T., Kimura, K., Sobrin, L., Connor, K.M., Sakoda, Y., Tamada, K., Ikeda, T., Sonoda, K.-H., Schunck, W.-H., 2015. Dietary omega-3 fatty acids suppress experimental autoimmune uveitis in association with inhibition of Th1 and Th17 cell function. PLoS ONE 10 (9), e0138241. https://doi.org/10.1371/journal.pone.0138241.

Siew, A., Le, H., Thiovolet, M., Gellert, P., Schatzlein, A., Uchegbu, I., 2012. Enhanced oral absorption of hydrophobic and hydrophilic drugs using quaternary ammonium palmitoyl glycol chitosan nanoparticles. Mol. Pharm. 9 (1), 14–28. https://doi.org/10.1021/mp200469a.

Squires, H., Poku, E., Bermejo, I., Cooper, K., Stevens, J., Hamilton, J., Wong, R., Denniston, A., Pearce, I., Quhill, F., 2017. A systematic review and economic evaluation of adalimumab and dexamethasone for treating non-infectious intermediate uveitis, posterior uveitis or panuveitis in adults. Health Technol. Assess. (Rockv) 21, 1–170. https://doi.org/10.3310/hta21680.

Srinivasan, B., Kolli, A.R., Esch, M.B., Abaci, H.E., Shuler, M.L., Hickman, J.J., 2015. TEER measurement techniques for in vitro barrier model systems. J. Lab. Autom. 20 (2), 107–126. https://doi.org/10.1177/2211068214561025.

Strandvik, G.F., 2009. Hypertonic saline in critical care: A review of the literature and guidelines for use in hypotensive states and raised intracranial pressure. Anaesthesia. 64, 990–1003. https://doi.org/10.1111/j.1365-2044.2009.05986.x.

Sun, D., Liang, D., Kaplan, H.J., Shao, H., 2015. The role of Th17-associated cytokines in the pathogenesis of experimental autoimmune uveitis (EAU). Cytokine 74 (1), 76–80. https://doi.org/10.1016/j.cyto.2014.12.017.

Tan, H.Y., Agarwal, A., Lee, C.S., Chhablani, J., Gupta, V., Khatri, M., Nirmal, J., Pavesio, C., Agrawal, R., 2016. Management of noninfectious posterior uveitis with intravitreal drug therapy. Clin. Ophthalmol. 10, 1983–2020. https://doi.org/10.2147/OPTH.S89341.

The Association for Research in Vision and Ophthalmology- Statement for the Use of Animals in Ophthalmic and Vision Research, (n.d.). https://www.arvo.org/About/policies/statement-for-the-use-of-animals-in-ophthalmic-and-vision-research/ (accessed March 21, 2020).

Toshida, H., Nguyen, D.H., Beuerman, R.W., Murakami, A., 2009. Neurologic evaluation of acute lacrimomimetic effect of cyclosporine in an experimental rabbit dry eye model. Investig. Ophthalmol. Vis. Sci. 50, 2736–2741. https://doi.org/10.1167/iovs.08-1880.

Uchegbu, I.F., Breznikar, J., Zaffalon, A., Odunze, U., Schätzlein, A.G., 2021. Polymeric Micelles for the Enhanced Deposition of Hydrophobic Drugs into Ocular Tissues, without Plasma Exposure. Pharmaceutics 13, 744. https://doi.org/10.3390/pharmaceutics13050744.

Uy, H.S., Yu-Keh, E., Chan, P.S., 2015. Posterior uveitis. Dev. Ophthalmol. 55, 163–166. https://doi.org/10.1159/000438968.

Watson, C., Mahe, M., Helmrath, M., 2015. In vivo Fluorescein Isothiocyanate-dextran (FD4) Permeability Assay. BIO-PROTOCOL. 5 https://doi.org/10.21769/BioProtoc.1618.

Ye, D., Dawson, K.A., Lynch, I., 2015. A TEM protocol for quality assurance of in vitro cellular barrier models and its application to the assessment of nanoparticle transport mechanisms across barriers. Analyst. 140 (1), 83–97.